# **ORGANOMETALLICS**

pubs.acs.org/Organometallics Article

# Anisotropic $\pi$ Bonding in Bis(iminoxolene)ruthenium: Consequences for Alkene and Alkyne Binding

Patricia Rose H. Ayson and Seth N. Brown\*



Cite This: Organometallics 2024, 43, 1889–1903



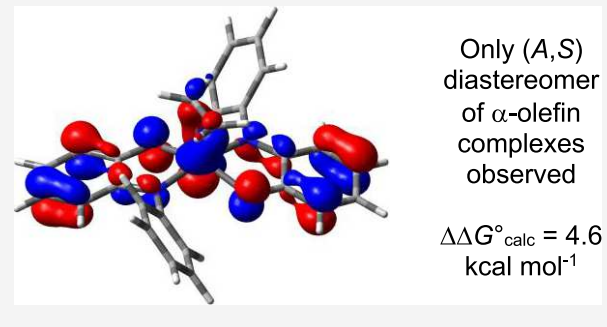
**ACCESS** I

III Metrics & More

Article Recommendations

Supporting Information

**ABSTRACT:** Orientational preferences in alkene and alkyne complexes arise from differences in the  $\pi$  backbonding capabilities of the relevant  $\mathrm{d}\pi$  orbitals, which typically are engendered by an unsymmetrical arrangement of ancillary ligands. The metal trans-bis-(iminoxolene) fragment is  $C_2$ -symmetric but discriminates between perpendicular  $\mathrm{d}\pi$  orbitals because only one of them has a strong  $\pi$  interaction with the iminoxolenes. To assess this effect, square pyramidal bis(iminoxolene) alkene and alkyne complexes (Diso) $_2$ Ru(L) (Diso = N-(2,6-diisopropylphenyl)-4,6-di-tert-butyl-o-iminobenzoquinone) are prepared via the bis-acetonitrile complex cis-(Diso) $_2$ Ru-(NCCH $_3$ ) $_2$ . The alkenes and alkynes align roughly along the O–Ru–O



axis but are turned slightly toward the cleft between the iminoxolene ligands, which orients the ligand  $\pi^*$  orbital with the  $d\pi$  orbital that is not engaged in bonding with the iminoxolenes. In the alkyne complexes,  $\pi$  donation from the alkyne competes effectively with the ruthenium-iminoxolene  $\pi$  bonding, forming a favorable four-electron, three-orbital system. The barrier to rotation in the 1-hexyne complex is 19.0 kcal mol<sup>-1</sup>, while allylbenzene dissociates more readily than it undergoes rotation, with a barrier of 17.4 kcal mol<sup>-1</sup>. The strong orientational preference leads to high facial selectivity of alkene binding, with only one diastereomer of the 1-alkene adducts observed by NMR (>30:1 selectivity).

# ■ INTRODUCTION

In the bonding of alkenes and alkynes to transition metals,  $\pi$  interactions play a major role. For both classes of ligands, backbonding of filled  $d\pi$  orbitals into empty carbon—carbon  $\pi^*$  orbitals usually contributes significantly to the energetics of binding. Alkynes may also have a  $\pi$  donor interaction from the alkyne  $\pi$  bonding orbital perpendicular to the metal—alkyne plane.

The presence of  $\pi$  bonding introduces the possibility of electronically driven orientational preferences and corresponding barriers to rotation. If the two possible  $d\pi$  orbitals that can potentially backbond ( $d_{xz}$  and  $d_{yz}$ , if the z-axis is taken as the vector between the metal and the centroid of the alkene or alkyne) are degenerate, as in axially symmetric compounds such as  $W(CO)_5$  (alkene),<sup>3</sup> then there is no difference in the energetics of  $\pi$  bonding with respect to orientation and barriers to rotation are small.4 Engendering a preferred orientation requires an unsymmetrical coordination sphere, where the degree of orientational preference depends on the electronic differentiation between the  $d_{xz}$  and  $d_{vz}$  orbitals. For example, in the pseudo-octahedral d<sup>6</sup> mononitrosyl complex [CpRe(NO)- $(PPh_3)(C_2H_4)^{-1}$ , the alkene prefers to have its C-C bond perpendicular to the nitrosyl linkage, allowing it to backbond with the  $d\pi$  orbital that is not also backbonding to the strongly  $\pi$  accepting nitrosyl (Figure 1). The barrier to alkene rotation is 16.4 kcal mol<sup>-1</sup> (369 K). When the asymmetry between  $d\pi$ orbitals is less, as when the weaker  $\pi$  acceptor CO is present in

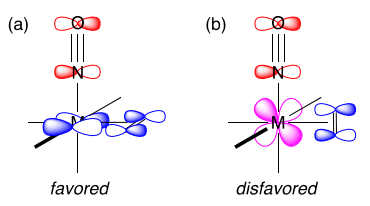


**Figure 1.** Possible alkene orientations in an octahedral  $d^6$  mononitrosyl complex. (a) Favored orientation, where the backbonding  $d\pi$  orbital does not interact with the nitrosyl. (b) Disfavored orientation, where backbonding to the alkene takes place from a  $d\pi$  orbital that is also backbonding to the strongly  $\pi$ -accepting nitrosyl ligand.

TpRe(CO)(PMe<sub>3</sub>)(C<sub>2</sub>H<sub>4</sub>), the rotation barrier is correspondingly lower ( $\Delta G^{\ddagger} = 10.0 \text{ kcal mol}^{-1}$ ).<sup>6</sup> In an extreme case, in octahedral d²-monooxo complexes, only the d orbital of  $\delta$  symmetry with respect to the oxo group is occupied, so backbonding to the alkene is only possible if its C–C bond is perpendicular to the M=O bond. Accordingly, the tungsten-

Received: June 16, 2024 Revised: July 26, 2024 Accepted: August 5, 2024 Published: August 10, 2024





(IV) complex  $W(O)(PMePh_2)_2Cl_2(C_2H_4)$  is rigid on the NMR time scale up to 353 K,<sup>7</sup> with a barrier to rotation of over 20 kcal mol<sup>-1</sup>.<sup>8</sup>

A strong orientational preference can foster enantiofacially selective binding of prochiral alkenes, if it forces the alkene substituents in one of the diastereomeric complexes into sterically unfavorable positions in order to maintain the electronically favored orientation. For example, complexes of the diastereomers of monosubstituted alkene complexes  $[\text{CpRe(NO)(PPh_3)(RCH=CH_2)}]^+$  maintain nearly identical core geometries, forcing the alkene substituent to approach either the nitrosyl or the cyclopentadienyl substituent. The former diastereomer is favored thermodynamically, by 32:1 in the cyclopentadienyl complex on the pentamethylcyclopentadienyl complex of 1-pentene.

Often, privileged structures that can give rise to high enantioselectivity in binding or reactivity have  $C_2$  symmetry. This point group is not readily compatible with the unsymmetrical structures described above that favor strong orientational preferences in alkene binding. A potential exception to this generalization would be the *trans*-bis-(iminoxolene) metal fragment (Figure 2), where the

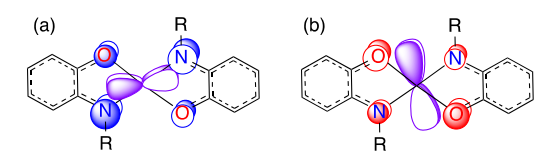


**Figure 2.** Filled  $\pi$  orbitals in the  $C_2$ -symmetric *trans*-bis-(iminoxolene)metal moiety, viewed down the 2-fold axis. (a) Strongly bonding combination of metal  $d\pi$  orbital with B-symmetry RAO combination. (b) Modestly antibonding combination of metal  $d\pi$  orbital with B-symmetry SJO combination.

particularities of the metal-ligand  $\pi$  bonding discriminate between the two d orbitals that are of  $\pi$  symmetry with respect to the  $C_2$  axis. One of the d orbitals, aligned roughly along the axis connecting the two iminoxolenes, interacts strongly with the B-symmetry combination of the frontier iminoxolene  $\pi$ orbitals, the so-called redox-active orbital (RAO). The RAO is quite close in energy to the d orbitals of elements in the middle of the d block, 13 so the interaction forms a bonding combination (Figure 2a) that is typically filled and an antibonding combination that is typically empty. In contrast, the d orbital aligned roughly between the iminoxolenes does not overlap with the RAO combinations, but rather is raised in energy by its antibonding interaction with the lower-lying ligand  $\pi$  orbital with out-of-phase oxygen and nitrogen p orbitals<sup>14</sup> (the so-called subjacent orbital or SJO<sup>15</sup>). This filled, high-energy orbital should thus be much better suited to backbonding than the lower-lying  $\pi$  bonding orbital (which also has significantly less metal character). The effects of the  $\pi$ anisotropy of the trans-bis(iminoxolene) fragment have been documented in the spectroscopy 16,17 and reactivity 18 of oxoosmium complexes.

Here we describe the preparation of a reduced *cis*-bis(iminoxolene)ruthenium bis(acetonitrile) complex that serves as a precursor for five-coordinate *trans*-bis-(iminoxolene)ruthenium complexes of alkynes and monosubstituted alkenes. Structural studies confirm that the unsaturated ligands are aligned to maximize backbonding from the higherenergy  $d\pi$  orbital. Dynamic NMR studies show that there are large barriers to rotation for both alkenes and alkynes,

indicating a strong preference for one particular orientation of the alkene or alkyne. Consonant with this, only one diastereomer is observed by <sup>1</sup>H NMR spectroscopy in complexes with monosubstituted alkenes.

#### ■ RESULTS AND DISCUSSION

Synthesis and Characterization of a *cis*-Bis-(iminoxolene)ruthenium Bis(acetonitrile) Complex. The neutral bis(iminoxolene)ruthenium complex (Diso)<sub>2</sub>Ru-(PPh<sub>3</sub>) (Diso = N-(2,6-diisopropylphenyl)-4,6-di-*tert*-butyl-o-iminobenzoquinone) may be prepared by two-electron reduction of (Diso)<sub>2</sub>RuCl<sub>2</sub> followed by the addition of triphenylphosphine. In the case of the alkene and alkyne adducts, it is more synthetically convenient to prepare an isolable precursor with volatile, labile ligands, namely *cis*-(Diso)<sub>2</sub>Ru(NCCH<sub>3</sub>)<sub>2</sub> (eq 1). The synthesis is achieved by

cobaltocene reduction of either *cis*- or *trans*-(Diso)<sub>2</sub>RuCl<sub>2</sub>, which appears to generate diamagnetic,  $C_2$ -symmetric [(Diso)<sub>2</sub>RuCl]<sup>-</sup> in solution. Addition of excess acetonitrile to the chloro anion generated in situ affords the crystalline neutral bis(acetonitrile) complex in good yield. The compound is *cis* in solution, as shown by the symmetry of its NMR spectra (for example, two isopropyl methine signals are seen rather than the one expected for the  $C_{2h}$ -symmetric *trans* isomer).

The cis geometry is confirmed by the solid-state structure of (Diso)<sub>2</sub>Ru(NCCH<sub>3</sub>)<sub>2</sub>·2CH<sub>3</sub>CN (Table S1 and Figure 3). The intraligand distances in iminoxolene groups are informative because they respond systematically to the electron density in the ligand redox-active orbital (RAO) and can be analyzed to provide an estimate of the apparent or metrical oxidation state (MOS).<sup>20</sup> cis-(Diso)<sub>2</sub>Ru(NCCH<sub>3</sub>)<sub>2</sub> displays an MOS of -1.28(5) for each iminoxolene ligand (Table 1). Compared to the MOS value of -0.78(4) per iminoxolene in cis-(Diso)<sub>2</sub>RuCl<sub>2</sub>, this indicates that the overall two-electron reduction of the dichloride complex is split equally between reduction of the metal and of the ligands, consistent with a highly covalent ruthenium-iminoxolene interaction. Indeed, the observed MOS value is close to the value of -1.34predicted for a complex with a  $\pi$  bond order of 0.5 per iminoxolene.13

Formation of both *trans* and *cis* isomers is precedented for bis(iminoxolene)ruthenium or -osmium complexes with two neutral donor ligands. <sup>18</sup> In the case of isoelectronic (Diso)<sub>2</sub>Ir-(py)Cl, both the *cis* and *trans* isomers are observed, with the *cis* isomer favored by 6.1 kcal mol<sup>-1.21</sup> The greater stability of the

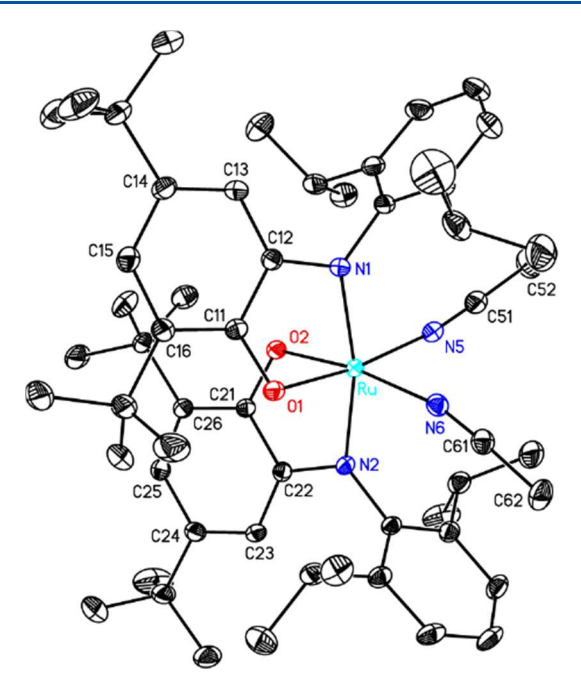


**Figure 3.** Thermal ellispoid plot of *cis*-(Diso)<sub>2</sub>Ru(NCCH<sub>3</sub>)<sub>2</sub>· 2CH<sub>3</sub>CN. Hydrogen atoms and lattice solvents are omitted for clarity.

Table 1. Selected Distances (Å) and Metrical Oxidation States (MOS)<sup>20</sup> for cis-(Diso)<sub>2</sub>Ru(NCCH<sub>3</sub>)<sub>2</sub><sup>a</sup>

	X-ray	DFT
Ru-O1	2.0036(11)	2.025
Ru-N1	2.014(10)	2.050
Ru-N5	2.0376(14)	2.024
C51-N5	1.142(3)	1.157
O1-C11	1.326(3)	1.313
N1-C12	1.368(5)	1.370
C11-C12	1.432(2)	1.441
C12-C13	1.416(2)	1.418
C13-C14	1.377(3)	1.383
C14-C15	1.419(5)	1.414
C15-C16	1.384(2)	1.385
C16-C11	1.423(5)	1.412
MOS	-1.28(5)	-1.24(7)

"Values in roman type are measured crystallographically; values in italics are from DFT calculations (B3LYP, SDD basis set for Ru and 6-31G\* basis set for other atoms) on the complex with *tert*-butyl, isopropyl, and methyl groups replaced with hydrogen atoms. Metrical data are averaged among chemically equivalent values, with stated esd's reflecting both the variance in the measured values and the statistical uncertainty of the crystallographic model.

cis isomer is attributed to steric effects, with electronic effects favoring the *trans* isomer, as judged by the greater computed stability of the *trans* isomer of unhindered  $(ap)_2Ir(py)Cl$   $(ap = 1,2-C_6H_4(O)(NPh))$ . A similar explanation likely holds for the ruthenium bis(acetonitrile) complex, as the simplified model hydrogen cyanide complex *trans*- $(ap)_2Ru(NCH)_2$  is calculated to be 2.0 kcal mol<sup>-1</sup> more stable than the *cis* isomer.

As has been seen in previously prepared *cis*-bis-(iminoxolene)ruthenium bipyridine complexes, <sup>22</sup> the optical spectrum of *cis*-(Diso)<sub>2</sub>Ru(NCCH<sub>3</sub>)<sub>2</sub> features a prominent, intense absorption in the near-IR ( $\lambda_{\text{max}} = 1084$  nm, Figure S20). With the aid of TDDFT calculations, this band is attributed to a HOMO (*B*-symmetry RAO nonbonding

orbital) to LUMO (A-symmetry Ru–RAO  $\pi^*$  orbital) transition (Figure 4). The Ru–RAO  $\pi$  bonding orbital is identified as the HOMO–4 orbital, with the  $\pi \to \pi^*$  transition assigned to the 420 nm band.

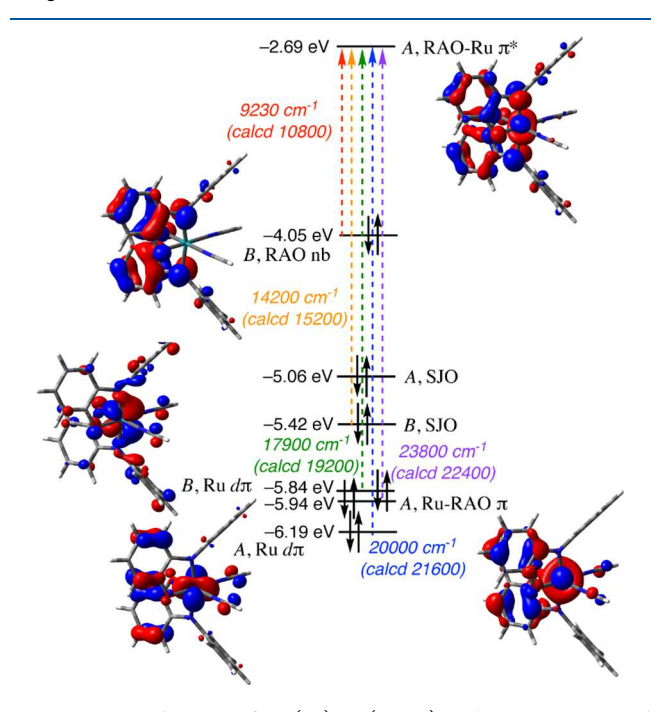


**Figure 4.** MO diagram of *cis*-(ap)<sub>2</sub>Ru(NCH)<sub>2</sub>. The HOMO-1 and HOMO-2, which are principally ligand in character, are not pictured.

The orbitals identified as principally Ru  $d\pi$  in character, notably the B-symmetry HOMO-3 and A-symmetry HOMO-5, show some degree of backbonding to the  $\pi^*$ orbitals of the nitrile ligands. This apparent mild  $\pi$  basicity of the cis-(Diso)<sub>2</sub>Ru fragment is consistent with its IR spectrum, where the nitrile stretches are observed at 2275 cm<sup>-1</sup>, only slightly raised over the free ligand (2268 cm<sup>-1</sup> in the gas phase<sup>23</sup>) and consistent with a modestly backbonding ruthenium center (similar to the 2276 cm<sup>-1</sup> observed for [CpRu(PMe<sub>3</sub>)(NCCH<sub>3</sub>)<sub>2</sub>]<sup>+</sup>). A useful comparison is *cis*-(acac)<sub>2</sub>Ru(NCCH<sub>3</sub>)<sub>2</sub>, which shares the same charge and geometry with (Diso)<sub>2</sub>Ru(NCCH<sub>3</sub>)<sub>2</sub> and also has oxygen donors trans to acetonitrile. The acetylacetonate complex absorbs at 2250 cm<sup>-1</sup>,<sup>25</sup> slightly lower than the iminoxolene complex (for reference,  $(acac)_2 Ru(CO)_2$  has  $\nu_{CO} = 2056$ , 1988 cm<sup>-1</sup>).<sup>26</sup> The fact that the (acac)<sub>2</sub>Ru fragment is a slightly better  $\pi$  donor than (Diso)<sub>2</sub>Ru is consistent with the ability of the iminoxolenes to withdraw electron density from the metal center as  $\pi$  acceptors themselves.

NMR spectra of cis-(Diso) $_2$ Ru(NCCH $_3$ ) $_2$  at ambient temperatures show distinct signals for bound and free acetonitrile, but these signals broaden and coalesce as the temperature is raised, indicating facile ligand exchange (Figure S22). Exchange is dissociative, as the line width of the bound  $CH_3$ CN peak is unaffected by the concentration of free  $CH_3$ CN. Dissociative exchange is also consistent with the activation parameters determined by Eyring analysis of the dynamic NMR data (Figure S23), with  $\Delta H^{\ddagger} = 20.3(5)$  kcal mol $^{-1}$  and  $\Delta S^{\ddagger} = 9.6(13)$  cal mol $^{-1}$  K $^{-1}$ . The extrapolated  $\Delta G^{\ddagger}$  at 298 K, 17.4 kcal mol $^{-1}$ , corresponds to a rate constant for exchange of about 1 s $^{-1}$  at 298 K. This is about  $10^5$  times faster than acetonitrile exchange in cis-(acac) $_2$ Ru(NCCH $_3$ ) $_2$ . Note

that the peaks due to the iminoxolenes in the complex are not affected by the dissociation of acetonitrile. This indicates that reassociation of acetonitrile to the five-coordinate intermediate must be faster than formation of trans-(Diso)<sub>2</sub>Ru(NCCH<sub>3</sub>)<sub>2</sub> from that intermediate. Such stereoretentive ligand exchange is also observed for cis-(Diso)<sub>2</sub>Ir(py)Cl.<sup>21</sup>

Preparation and Characterization of Five-Coordinate Alkene and Alkyne Complexes. Treatment of *cis*-(Diso)<sub>2</sub>Ru(NCCH<sub>3</sub>)<sub>2</sub> with monosubstituted alkenes such as 1-hexene or allylbenzene, or alkynes such as 1-hexyne, results in displacement of acetonitrile and formation of five-coordinate ruthenium complexes (eqs 2–3). Coordination of a second

equivalent of alkene or alkyne is not observed even in the presence of a large excess of ligand. The internal alkynes 3-hexyne and diphenylacetylene react similarly to 1-hexyne, but the internal alkene 2-hexene binds only weakly, partially displacing acetonitrile from  $(Diso)_2Ru(NCCH_3)_2$ , and stilbene does not react at all. Allylbenzene and 1-hexene bind with similar affinities  $(K_4 = 0.56$  for displacement of allylbenzene by 1-hexene in  $CD_2Cl_2$  at 293 K, eq 4). Alkynes bind more

strongly than alkenes, with 3-hexyne quantitatively displacing allylbenzene from (Diso)<sub>2</sub>Ru(CH<sub>2</sub>=CHCH<sub>2</sub>Ph).

NMR spectroscopy of the alkene and alkyne complexes show that the two iminoxolene ligands are inequivalent ( $C_1$ symmetry), consistent with slow rotation of the alkene or alkyne ligand. The alkene hydrogens appear at very disparate chemical shifts, with the 2-H and the cis-1-H resonating at approximately 5 ppm, while the trans-1-H appears far upfield  $(\delta 1.83 \text{ in } (\text{Diso})_2 \text{Ru}(\text{CH}_2 = \text{CHBu}))$ . One of the allylic hydrogens also resonates at unusually high field ( $\delta$  0.13 for (Diso)<sub>2</sub>Ru(CH<sub>2</sub>=CHCHH'Pr)). Hydrogens in metal-alkene complexes typically appear upfield of their positions in the free alkenes, but the large difference in chemical shift between the two terminal alkene hydrogens, as well as the upfield shift of one of the diastereotopic allylic hydrogens, suggests that in these compounds the (Diso)<sub>2</sub>Ru fragment has a large magnetic anisotropy that dominates the observed chemical shifts. The <sup>13</sup>C NMR signals of terminal and internal alkene carbons of bound 1-hexene are observed at  $\delta$  61.3 and 75.7 ppm, respectively, in the typical region for bound olefins.

The terminal hydrogen of the 1-hexyne complex is observed at  $\delta$  7.73 ppm and the diastereotopic propargylic hydrogens at  $\delta$  2.92 and 3.16 ppm ( $^2J$  = 17.1 Hz) in the  $^1H$  NMR spectrum. As measured by single- and multiple-bond  $^1H$ — $^{13}C$  correlation spectroscopy, the terminal alkyne carbon resonates at 116.2 and the internal carbon at 140.0 ppm. Formation of metal vinylidenes from terminal alkynes is well precedented for ruthenium,  $^{27}$  but the  $\alpha$  carbons of ruthenium vinylidenes invariably resonate downfield of 250 ppm,  $^{28}$  so the data for the present compound rule out vinylidene formation and are consistent with the presence of an intact alkyne. No C=C stretch could be observed in the IR spectrum of (Diso) $_2$ Ru-(HCCBu), presumably because of its low intensity. The alkyne stretch in (ap) $_2$ Ru(HCCH) is calculated to be at a scaled  $^{29}$  frequency of 1669 cm $^{-1}$ .

Structure and Bonding in Bis-Iminoxolene Ruthenium Alkyne and Alkene Complexes. The  $(\text{Diso})_2\text{Ru}$  complexes of 1-hexene, allylbenzene, and 3-hexyne all crystallize as five-coordinate monomers (Figure 5) that are well described as square pyramids with the  $\eta^2$  ligands in the apical position (Reedijk  $\tau$  values<sup>30</sup> close to zero, Table 2). The orientations of the unsaturated ligands in the alkene and alkyne complexes, as determined by X-ray crystallography, are strikingly similar (Figure 5). In each case the bound C–C bond is roughly aligned with the O–Ru–O axis, but canted slightly toward the cleft between the two iminoxolene ligands,

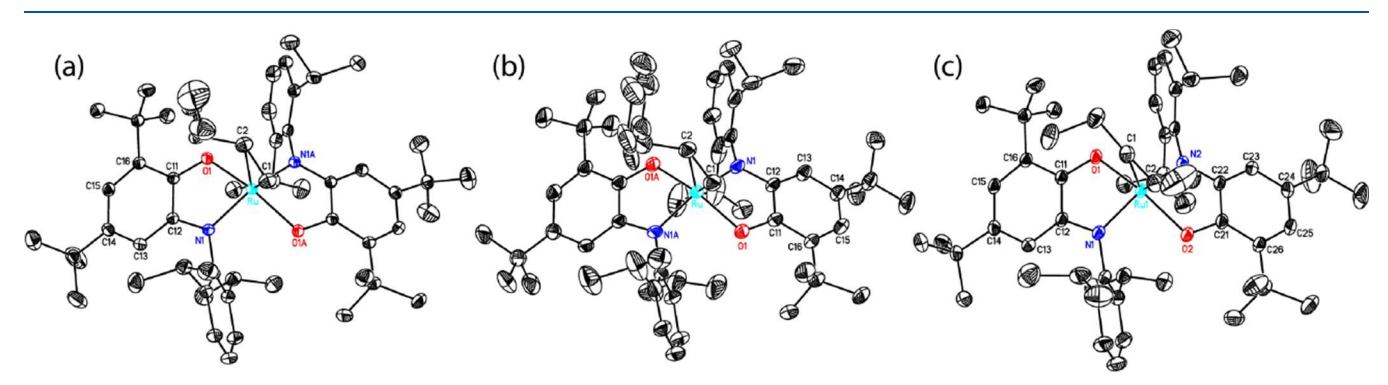


Figure 5. Thermal ellipsoid plots of (a)  $(Diso)_2Ru(CH_2=CHBu)$ ; (b)  $(Diso)_2Ru(CH_2=CHCH_2Ph)$ ; and (c)  $(Diso)_2Ru(EtC\equiv CEt)$ . Hydrogen atoms, lattice solvents, and minor components of disordered groups are omitted for clarity. Only one of the two crystallographically inequivalent molecules of  $(Diso)_2Ru(EtC\equiv CEt)$  is shown.

Table 2. Selected Distances (Å), Dihedral Angles (deg), Metrical Oxidation States (MOS) per Iminoxolene Ligand, <sup>20</sup> and  $\tau$  Values <sup>30</sup> for Bis(iminoxolene)ruthenium Alkene and Alkyne complexes <sup>a</sup>

	(Diso) <sub>2</sub> Ru (CH <sub>2</sub> =CHBu) X-ray	(Diso) <sub>2</sub> Ru (CH <sub>2</sub> =CHCH <sub>2</sub> Ph) X-ray	$(ap)_2$ Ru $(CH_2=CH_2)$ DFT	(Diso)₂Ru (EtC≡CEt) X-ray <sup>b</sup>	(ap)₂Ru (HC≡CH) DFT
Ru-O1	2.0399(13)	2.027(2)	2.035	2.042(4)	2.048
Ru-N1	1.9427(16)	1.943(3)	2.008	1.930(4)	1.963
Ru-C1	2.134(13)	2.130(24)	2.133	2.030(5)	2.044
Ru-C2	2.174(12)	2.151(19)			
C1-C2	1.410(6)	1.393(9)	1.419	1.265(3)	1.275
O1-C11	1.317(2)	1.316(4)	1.310	1.327(2)	1.319
N1-C12	1.385(2)	1.382(4)	1.373	1.398(3)	1.391
C11-C12	1.419(3)	1.419(4)	1.434	1.411(4)	1.424
C12-C13	1.405(3)	1.407(4)	1.418	1.403(4)	1.411
C13-C14	1.378(3)	1.372(4)	1.382	1.382(6)	1.387
C14-C15	1.417(3)	1.417(5)	1.415	1.409(6)	1.409
C15-C16	1.386(3)	1.381(5)	1.383	1.391(3)	1.387
C16-C11	1.431(3)	1.426(4)	1.413	1.419(3)	1.409
O1-Ru-C1-C2	-19.4	-15.5	-27.6	-5.5	-15.1
MOS	-1.36(9)	-1.33(8)	-1.26(7)	-1.56(10)	-1.46(9)
τ	0.13	0.10	0.19	0.20	0.09

<sup>&</sup>quot;Crystallographically determined values for  $(Diso)_2Ru(L)$  are given in roman type, while those calculated by DFT on  $(ap)_2Ru(L)$  are given in italic type. "Values are averaged among chemically equivalent instances in the two crystallographically inequivalent molecules in the unit cell. Esd's reflect both the statistically estimated uncertainties and the variance in the measured values.

with O–Ru–C1–C2 dihedral angles of roughly 15° (Table 2). This is doubtless an electronic effect, as it is also observed computationally with unhindered N-phenyl groups and ethene or ethyne ligands. It is consistent with an orientation that maximizes backbonding, lining up the ligand  $\pi^*$  orbital with position of the high-energy  $d\pi$  orbital in, for example,  $(Diso)_2Ru(PPh_3)$ .

Structurally, signatures for backbonding to alkenes include the carbon–carbon distance (elongated with greater backbonding) and the metal–carbon distances (shortened with greater backbonding). Structural data on neutral ruthenium complexes of unchelated monosubstituted alkenes that do not have strongly electron-withdrawing substituents (Table S2) are very similar to those shown by  $(Diso)_2Ru(1-alkene)$  complexes, suggesting that the  $(Diso)_2Ru$  fragment is similar in its backbonding abilities to other neutral low-valent Ru fragments such as  $Cp*Ru(\eta^3-allyl)$ .

In alkyne complexes, both backbonding to the alkyne  $\pi^*$  and  $\pi$  donation from the alkyne  $\pi_{\perp}$  orbital have distinctive structural and spectroscopic indicia. Backbonding elongates the C $\equiv$ C bond and decreases the alkyne stretching frequency; these metrics do not appear to be sensitive to the extent of  $\pi$  donation of the alkyne.<sup>32,33</sup> In (Diso)<sub>2</sub>Ru(HC $\equiv$ CBu), the C $\equiv$ C stretch could not be located in the IR, but the C $\equiv$ C distance of 1.265(3) Å is typical of ruthenium alkyne complexes (Table S3), such as for example Cp\*Ru( $\eta^3$ -C<sub>3</sub>H<sub>5</sub>)(PhC $\equiv$ CPh), d(C $\equiv$ C) = 1.261(3) Å.<sup>34</sup>

Alkyne  $\pi$  donation to the metal is marked by shortened metal—carbon distances and by downfield shifts in the <sup>13</sup>C NMR resonances of the alkyne carbons.<sup>2</sup> Both of these metrics appear to scale with the degree of  $\pi$  donation. For example, in complexes of Mo and W, two-electron donor alkynes resonate at  $\sim \delta$  120 ppm<sup>35</sup> and have metal—carbon distances of  $\sim$ 2.14 Å, while four-electron donor alkynes resonate at  $\sim \delta$  200 ppm and have metal—carbon distances of  $\sim$ 2.03 Å. When one  $\pi$  bond is shared between two alkynes donating to a single metal d orbital (a so-called 3-electron donor alkyne), the metrics are almost exactly halfway in between, with  $\delta \sim$  160 ppm and

 $d(M-C)\approx 2.09$  Å. This scaling also appears to apply in cases where competition is not required by symmetry to be equal. For example, in W(IV) oxo-alkyne complexes, the alkyne invariably lies perpendicular to the M=O vector, so the alkyne  $\pi_{\perp}$  orbital competes with one of the oxygen  $p_{\pi}$  orbitals to donate to an empty metal  $d\pi$  orbital. In such complexes,  $\delta(^{13}C)=159(8)$  ppm and d(W-C)=2.094(15) (Table S4). These are indistinguishable from the values seen in bis(alkyne) complexes, so the alkyne competes on an equal footing with the oxo for  $\pi$  donation to the metal, leading to the characterization of these alkynes as three-electron donors.  $^{36,37}$ 

For reported two-electron donor alkyne complexes of ruthenium,  $\delta(^{13}C) = 82(12)$  ppm and d(Ru-C) = 2.18(5)Å, while four-electron alkyne complexes have  $\delta(^{13}C)$  = 140(10) ppm and d(Ru-C) = 2.06(4) Å (Table S3). The one structurally characterized ruthenium alkyne that could be considered to have a three-electron interaction has an intermediate Ru-C distance of 2.11 Å.38 According to these metrics, (Diso)<sub>2</sub>Ru(EtC≡CEt) appears very similar to literature examples of four-electron donor alkynes, with  $\delta(^{13}C)$ = 139.7 ppm and d(Ru-C) = 2.030(5) Å. However, the fact that the <sup>13</sup>C chemical shifts of the ruthenium alkyne complexes are so far upfield of those shown by four-electron donor alkynes in molybdenum and tungsten complexes, and to a lesser extent the longer ruthenium-carbon distances, suggests that  $\pi$  donation in the ruthenium alkynes is not as strong as it is in the group 6 complexes. In fact, all but one of the structurally characterized "four-electron donor" Ru alkyne complexes are of the form CpRuCl(RC≡CR'). 39,40 In contrast to the octahedral Mo(II) or W(II) complexes, where the d orbital into which the alkyne donates is strictly  $\pi$  in character, the d orbital in the two-legged piano stool complex has a  $\sigma^*$  interaction with the cyclopentadienyl group (see Figure S26 for the relevant molecular orbitals calculated for CpRuCl[HCCH]). This reduces the  $\pi$  bond order to the alkyne to the point where it looks spectroscopically and structurally similar to a three-electron donor alkyne on a group 6 metal. (The one nonpiano-stool "four-electron donor"

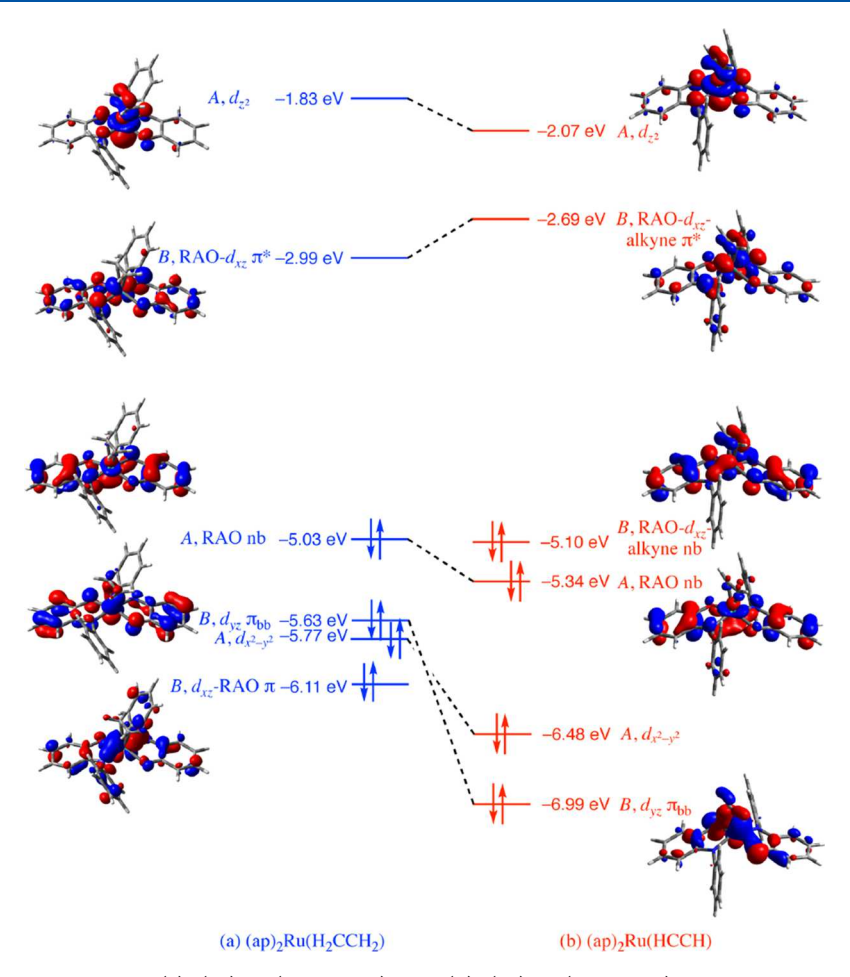


Figure 6. Molecular orbital diagrams for (a)  $(ap)_2Ru(H_2C=CH_2)$  and (b)  $(ap)_2Ru(HC\equiv CH)$ . Only orbitals with significant metal  $d\pi$  or iminoxolene RAO character are listed. The A-symmetry  $d_{x^2-y^2}$  orbitals are not pictured.

ruthenium complex, (MesPDI)Ru(HC $\equiv$ CH), <sup>41</sup> has an analogous issue with poor  $\pi$  bonding to the alkyne, as a square planar complex would not have an empty  $\pi$  orbital suitable for interacting with the alkyne. <sup>42</sup>) The structural and spectroscopic characterization of (Diso)<sub>2</sub>Ru(EtC $\equiv$ CEt) thus suggests not that the alkyne donates fully to the ruthenium, but rather that it competes about as effectively with the  $\pi$  donation from the iminoxolenes as it does with the  $\sigma$  bonding from the cyclopentadienyl ligand in CpRuCl(RC $\equiv$ CR').

This analysis agrees with the structural characteristics of the iminoxolene ligands. The alkene complexes have MOS values of -1.36(9) (hexene) and -1.33(8) (allylbenzene), close to the MOS value of -1.34 expected for a complex having an overall metal-iminoxolene  $\pi$  bond order of 1.0. In contrast, the MOS of the alkyne complex (Diso)<sub>2</sub>Ru(EtC≡CEt) is significantly more negative, at -1.56(10). This indicates that the metal-iminoxolene bonding orbital has shifted its electron density to be more on the ligand, consistent with donation from the alkyne  $\pi_{\perp}$  into this orbital. A similar effect is seen in a series of bis(iminoxolene)osmium compounds, where increasing the  $\pi$  donor ability of the ancillary ligands from dichloride to ethylene glycolate to oxo produces a change in MOS from -0.94 to -1.47 to -1.98. Quantitatively, one can use the correlation between  $\pi$  bond order and MOS in Ru iminoxolenes<sup>13</sup> to estimate that the overall Ru-iminoxolene  $\pi$  bond order in (Diso)<sub>2</sub>Ru(EtC $\equiv$ CEt) is 0.67. This suggests that  $\pi$  donation from the alkyne competes with that from the iminoxolene, but not quite on an equal footing. This is

consistent with the spectroscopic data, particularly the <sup>13</sup>C chemical shift, which is noticeably upfield of the <sup>13</sup>C shifts in three-electron donor alkynes.

Density functional theory calculations paint a picture of the bonding in the alkene and alkyne complexes that is in good agreement with this analysis (Figure 6). The B symmetry RAO combination is strongly engaged in  $\pi$  bonding with the Ru d<sub>xx</sub> orbital (the antibonding combination is the LUMO in both complexes), but in the acetylene complex this  $\pi$  interaction also involves the alkyne  $\pi_{\perp}$  orbital. This converts the interaction into a three-orbital, four-electron system, which has the result of raising the energy of the  $\pi^*$  orbital noticeably (relative to its position in the ethylene complex) and introducing a  $\pi_{nb}$  orbital as the HOMO of  $(ap)_2Ru(HC \equiv$ CH), with the significant participation of both the alkyne and iminoxolene  $\pi$  orbitals in this latter MO attesting to the competition of both ligands for  $\pi$  bonding as discussed above. In both complexes, the A-symmetry RAO combination is largely nonbonding, but shows some amount of  $\pi$  donation to the  $d_{z^2}$  orbital, which is relatively low in energy in these square pyramidal complexes (LUMO+1 in both compounds). As is typical of trans-bis-iminoxolene complexes, 43 the optical spectra show very intense absorptions in the red (Figure 7), which are assigned as A (RAO)  $\rightarrow B$  (RAO- $d_{xz}$   $\pi^*$ ) transitions. The absorption maxima predicted by TDDFT calculations (661 and 517 nm for the alkene and alkyne complexes, respectively) are in reasonable agreement with those observed experimentally (700 and 593 nm, respectively).

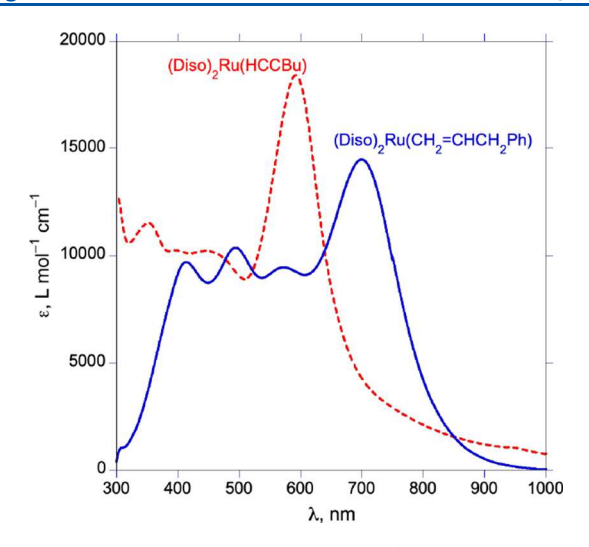


Figure 7. Optical spectra in toluene of  $(Diso)_2Ru(CH_2=CHCH_2Ph)$  (blue solid line) and  $(Diso)_2Ru(HC\equiv CBu)$  (red dashed line).

It is worth contrasting the bonding of the alkyne in (Diso)<sub>2</sub>Ru(RC≡CR) with that of the intramolecularly coordinated alkyne in  $(\kappa^2, \eta^2$ -Tipsi)(3,5- ${}^t$ Bu<sub>2</sub>Cat)IrCl (Tipsi = *N*-(2,6-bis(triisopropylsilylethynyl)phenyl)-4,6-di-*tert*-butyl-2imino-o-benzoquinone). Despite the fact that IrCl is nominally isoelectronic with Ru, the alkyne bonding in the two compounds is strikingly different. While the Ru compound shows both significant  $\pi$  backbonding to, and appreciable  $\pi$ donation from, the alkyne, the coordinated alkyne in the Ir compound is neither a significant donor nor acceptor of  $\pi$ electrons (a Polonius-type alkyne).<sup>44</sup> Two factors probably contribute to this stark difference in bonding. The first is that the mer geometry of the intramolecularly coordinated iminoxolene-alkyne ligand constrains the orientation of the alkyne so that its alignment with the relevant metal  $d\pi$  orbitals is suboptimal.

The second factor is that the iridium compound is notably more electron-poor than the ruthenium compound. This is due to the presence of one dioxolene ligand on the iridium compound, to the intrinsically higher electronegativity of the element farther to the right in the periodic table, and to the higher oxidation state of iridium compared to ruthenium required if the two elements are to have the same electron count. Clearly, the more electron-poor iridium center will be a poorer backbonder than ruthenium. It is less clear why alkyne-to-metal  $\pi$  donation should be diminished at an electron-poor center. Indeed, the limited data available suggest that  $\pi$  donation is not much affected intrinsically by moving to the right in the periodic table. For example, the octahedral tungsten(II) complex Tp\*W(CO)I(MeC $\equiv$ CMe) ( $\delta_{13C}$  avg. = 207.6)<sup>46</sup> appears to have very similar  $\pi$  donation compared to

the rhenium(III) complex TpReCl<sub>2</sub>(EtC $\equiv$ CEt) ( $\delta_{13C}$  = 212.9),<sup>47</sup> and the pseudotetrahedral tris(alkyne)tungsten(0) complex (EtC $\equiv$ CEt)<sub>3</sub>W(CO) ( $\delta_{13C}$  avg. = 181.0)<sup>36</sup> is very similar to the rhenium(I) complex [(EtC≡CEt)<sub>3</sub>Re(PMe<sub>3</sub>)]-OTf  $(\delta_{13C} \text{ avg.} = 173.6)$ . But the ability of an alkyne to compete with an oxo group does appear to diminish on moving to the right in the periodic table. Thus, the butyne ligand in the tungsten(IV) oxo-alkyne complex Tp\*W(O)I-(MeC $\equiv$ CMe) ( $\delta_{13C}$  avg. = 162.4)<sup>37</sup> appears to donate significantly more strongly than the butyne in the rhenium(V) oxo-alkyne complex Re(O)Me<sub>3</sub>(MeC $\equiv$ CMe) ( $\delta_{13C}$  = 143.5). 49 Possibly the poorer backbonding from the highervalent later metal (see, e.g.,  $\nu_{C \equiv C} = 1741 \text{ cm}^{-1}$  in [(EtC  $\equiv$  CEt)<sub>3</sub>Re(PMe<sub>3</sub>)]OTf<sup>49</sup> vs 1702 cm<sup>-1</sup> in (EtC  $\equiv$  CEt)<sub>3</sub>W- $(CO)^{50}$ ) contracts the C $\equiv$ C bond, lowering the energy of the  $\pi$  orbital and making it a poorer donor. In contrast, the  $\pi$ bonding to the oxo or iminoxolene ligand is strengthened as the d orbital energies of the metal fall, becoming closer to the energies of the oxygen- or nitrogen-containing orbitals.

**Energetics of Alkene and Alkyne Rotation.** The alkene or alkyne ligands bonded to Ru are aligned to maximize  $\pi$ backbonding, so rotation of the unsaturated ligand is expected to incur a significant energetic penalty. This is observed computationally in (ap)<sub>2</sub>Ru(H<sub>2</sub>C=CH<sub>2</sub>), which has a calculated  $\Delta G^{\ddagger} = 12.4 \text{ kcal mol}^{-1}$  for rotation of ethylene about the metal-centroid axis. In the transition state for bond rotation, the alkene is aligned so that it cannot backbond with the highlying Ru d $\pi$  orbital (Figure 8a), and structural data are consistent with an appreciable decrease in the degree of backbonding to the alkene (Table 3). In contrast to the calculated C<sub>2</sub>-symmetric equilibrium geometry, the transition state shows a slight distortion in the ruthenium-iminoxolene bonds, with Ru-O1 and -N2 bond lengths about 0.01 Å shorter than the Ru-O2 and -N1 bonds, consistent with the alkene becoming essentially a pure  $\sigma$  donor in the transition state and fostering a distortion like that observed in the phosphine complex (Diso)<sub>2</sub>Ru(PPh<sub>3</sub>).<sup>19</sup>

The orbital mismatch in the transition state is even more evident in the alkyne complex  $(ap)_2Ru(HC\equiv CH)$ . The HOMO is not backbonding but rather has an unfavorable filled–filled interaction with the alkyne  $\pi_{\perp}$  orbital (Figure 8b). Instead, it is the empty Ru–RAO  $\pi^*$  LUMO that can interact with the empty alkyne  $\pi^*$  (Figure 8c). The loss of backbonding in the transition state is marked by the contraction of the C $\equiv$  C bond (by 0.034 Å) and increase in the calculated C $\equiv$ C stretching frequency (from 1669 to 1811 cm $^{-1}$ ). The loss of  $\pi$  donation in the transition state is marked by the elongation of the Ru–C distances by 0.16 Å. The MOS values of the iminoxolenes also become significantly more positive, with the value of -1.15(9) consistent with a  $\sigma$ -only ligand lacking the  $\pi$  bonding that competes with the iminoxolene–metal  $\pi$ 

Table 3. Selected Parameters of the Calculated Transition States for Rotation of the Hydrocarbon Ligand in  $(ap)_2Ru(H_nCCH_n)$  (n = 1, 2)

parameter	$[(ap)_2Ru(H_2C = CH_2)]^{\ddagger}$	change from equilibrium geometry	$[(ap)_2Ru(HC{\equiv}CH)]^{\ddagger}$	change from equilibrium geometry
d(CC)	1.393 Å	−0.026 Å	1.241 Å	-0.034 Å
d(RuC)	2.218 Å	+0.085 Å	2.204 Å	+0.160 Å
$\phi$ (O1-Ru-C1-C2)	48.9°	+76.5°	53.2°	+68.3°
MOS	-1.18(8)	+0.08	-1.15(9)	+0.41
τ	0.16	-0.03	0.25	+0.16
$\Delta G^{\ddagger}$	12.4 kcal mol <sup>-1</sup>		$18.7 \text{ kcal mol}^{-1}$	

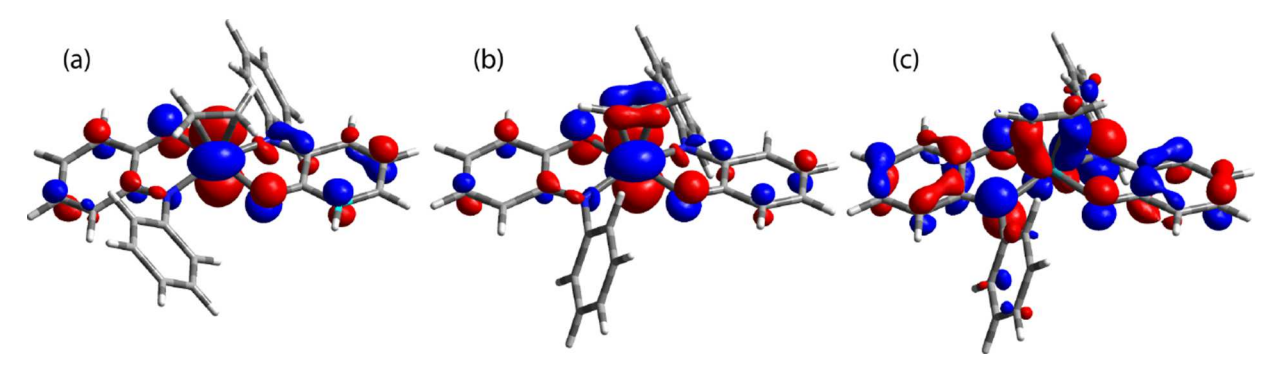


Figure 8. Selected Kohn–Sham orbitals calculated for the transition states for ligand rotations. (a) HOMO–1 of  $[(ap)_2Ru(H_2C=CH_2)]^{\ddagger}$ . (b) HOMO of  $[(ap)_2Ru(HC\equiv CH)]^{\ddagger}$ . (c) LUMO of  $[(ap)_2Ru(HC\equiv CH)]^{\ddagger}$ .

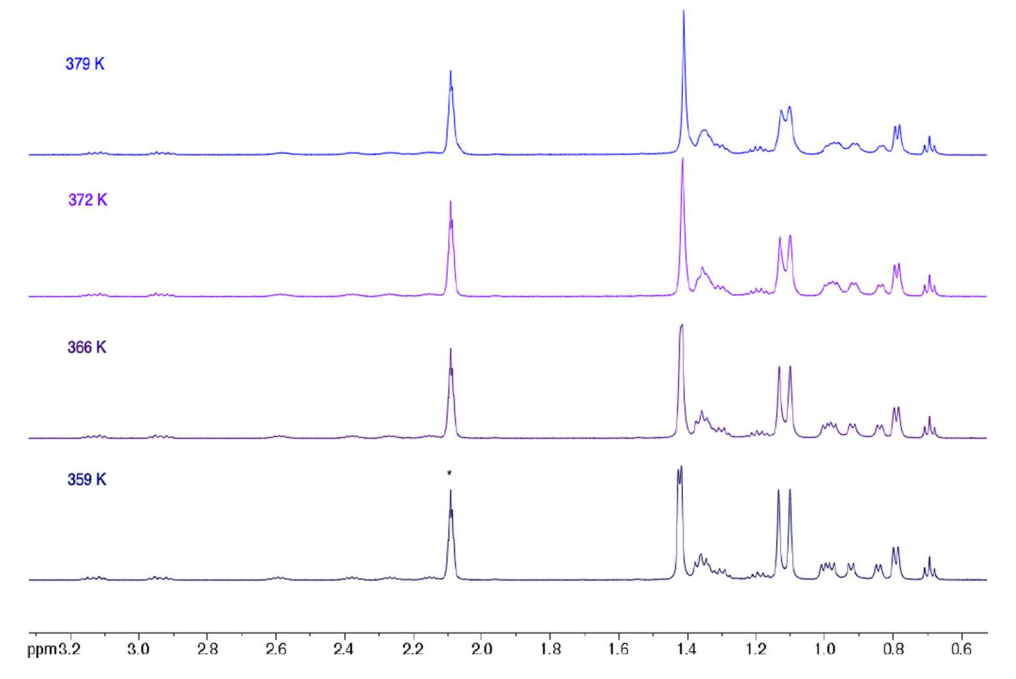


Figure 9. ¹H NMR spectra of (Diso)₂Ru(HC≡CBu) (toluene-d<sub>8</sub>, 500 MHz). The toluene residual peak at δ 2.09 ppm is marked with \*.

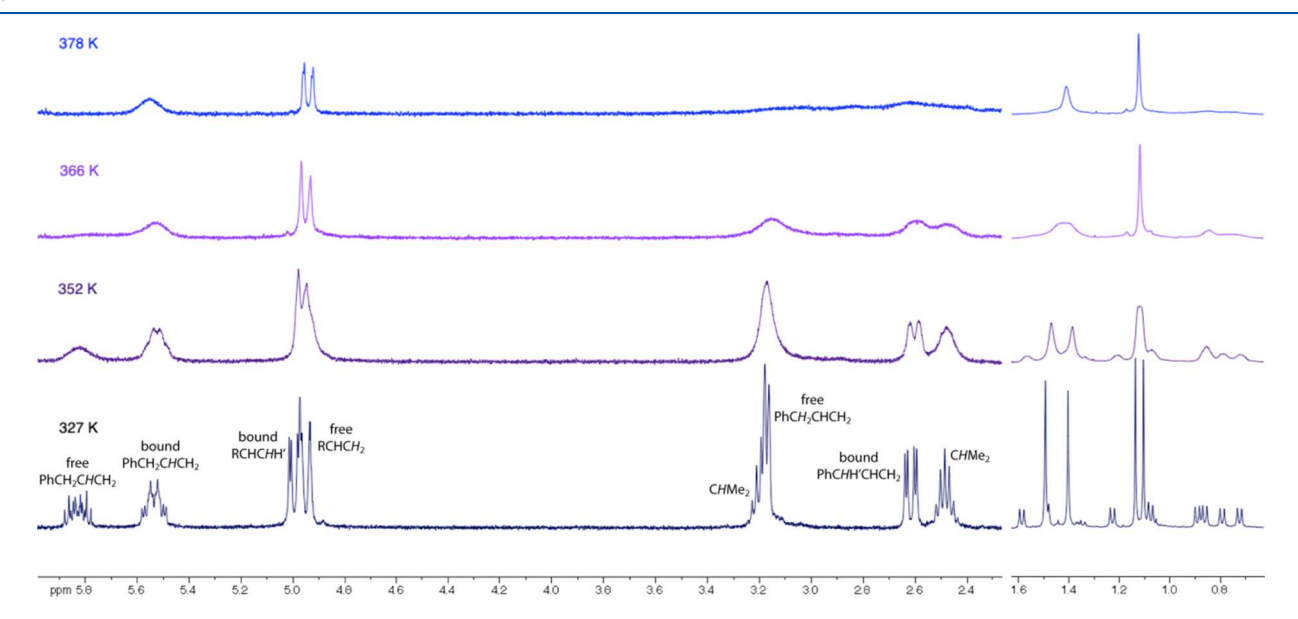


Figure 10.  $^{1}$ H NMR spectra of (Diso) $_{2}$ Ru(CH $_{2}$ =CHCH $_{2}$ Ph) in the presence of 0.4 equiv free CH $_{2}$ =CHCH $_{2}$ Ph (toluene- $d_{8}$ , 500 MHz). The vertical scale for the upfield region is reduced by a factor of 12 compared to the downfield region.

Table 4. Barriers to Rotation of Alkenes and Alkynes in Selected Complexes

compound	co-ligand or other factor governing alignment of alkene/alkyne	$\Delta G^{\ddagger}$ (kcal mol <sup>-1</sup> ) [T, K]	ref
alkene complexes			
$TpRe(CO)(PMe_3)(CH_2=CH_2)$	CO	10.0 [188]	6
trans-W(CO) <sub>4</sub> (CH <sub>2</sub> =CHBu) <sub>2</sub>	CH <sub>2</sub> =CHBu	11.3 [237]	52
$CpFe(CO)(SnMe_3)(CH_2=CH_2)$	CO	12.8 [223]	53
$(Me_3P)Pt(CH_2=CH_2)_2$	trigonal geometry	13.0 [269]	54
$[CpRe(NO)(PPh_3)(CH_2=CH_2)]BF_4$	NO	16.4 [369]	5
$(Diso)_2Ru(CH_2=CHCH_2Ph)$	iminoxolene $\pi$ bonding anisotropy	>17.3 [379]	this work
(Me <sub>2</sub> phen)PtI <sub>2</sub> (CH <sub>2</sub> =CHMe)	tbp geometry (equatorial alkene)	20.5 [383]	55
$W(O)Cl_2(CH_2=CH_2)(PMePh_2)_2$	O	>20 [353]	7
$[Cp_2W(H)(CH_2=CHCH_3)]PF_6$	Cp <sub>2</sub> wedge	23.6 [298]	56
alkyne complexes			
$(Me_2NCS_2)_2W(CO)(HC \equiv CH)$	CO	11.9 [246]	57
(Mes₂nacnac)Cu(PhC≡CH)	trigonal geometry	13.4 [263]	58
$(Me_2NCS_2)_2Mo(EtC \equiv CEt)_2$	EtC≡CEt	15.4 [373]	59
$(Me_2Phen)PtI_2(MeC \equiv CH)$	tbp geometry, equatorial alkyne	17.1 [333]	60
$CpW(CH_3)(CO)(HC \equiv CH)$	CO	18.2 [364]	61
$Tp*W(I)(CO)(HC \equiv CH)$	CO	18.6 [343]	62
$(Diso)_2Ru(HC \equiv CBu)$	iminoxolene $\pi$ bonding anisotropy	19.0 [379]	this work
$[CpRe(NO)(PPh_3)(EtC \equiv CEt)]BF_4$	NO	>22.6 [453]	63
$Tp*W(O)(I)(HC \equiv CH)$	O	>25 [433]	37

bonding. Consistent with weakening of both backbonding and  $\pi$  donation in the ethyne complex, the calculated rotation barrier of 18.7 kcal mol<sup>-1</sup> is greater than that in the ethene complex.

Experimentally, the barriers to rotation can be measured by dynamic NMR spectroscopy. The terminal alkyne complex (Diso)<sub>2</sub>Ru(HC $\equiv$ CBu) shows inequivalent iminoxolene ligands at room temperature, but the iminoxolene resonances broaden and coalesce at higher temperatures (Figure 9). The peaks due to the bound alkyne, such as the diastereotopic propargylic hydrogens at  $\delta$  2.9 and 3.1 ppm, are not affected by changing the temperature, nor does the presence of free alkyne affect the spectrum. These observations indicate that the dynamic process involves neither association nor dissociation of alkyne, consistent with its being a rotation of the alkyne ligand. The rate constant of 20 s<sup>-1</sup> at 379 K corresponds to  $\Delta G^{\ddagger} = 19.0$  kcal mol<sup>-1</sup>, in close agreement with the value calculated for (ap)<sub>2</sub>Ru(HC $\equiv$ CH).

The alkene complex (Diso)<sub>2</sub>Ru(CH<sub>2</sub>=CHCH<sub>2</sub>Ph) also shows exchange above 340 K between the two iminoxolene environments, which are inequivalent at room temperature (Figure 10). In contrast to the alkyne complex, iminoxolene exchange in the allylbenzene complex is concurrent with exchange between free and bound alkene. Quantitatively, the rate constant obtained from line shape analysis of the tert-butyl hydrogens  $(k_{\text{exch}})$  is consistently one-half the value of the dissociative rate constant obtained from analysis of the exchange of bound and free allylbenzene ( $k_{diss}$ ). This is most consistent with a mechanism where alkene dissociates to give a four-coordinate (Diso)<sub>2</sub>Ru intermediate. Rebinding of alkene would take place with an equal probability of the alkene C1 overlying either of the two iminoxolene ligands. This means that every dissociation event would always lead to exchange between bound and free alkene, but would only result in exchange between tert-butyl hydrogens half the time, accounting for the quantitative relationship between the two rate constants. Alkene rotation must take place much more slowly than alkene dissociation. Because alkene rotation would lead to tert-butyl group exchange but not exchange between

bound and free alkene, if alkene rotation took place at a significant rate, the rate constant for *tert*-butyl group exchange would be greater than half that of alkene dissociation.

The putative four-coordinate intermediate is calculated by DFT to have a square planar geometry. This suggests that alkene rebinding could take place not just with either possible orientation of the alkene, but also with either possible face of the intermediate. It was not possible to confirm this by dynamic NMR, but EXSY spectroscopy at 328 K clearly indicates that exchange proceeds through an intermediate with effective  $C_{2h}$  symmetry, with all four isopropyl methine hydrogens exchanging with each other and the isopropyl methyl doublets exchanging in two sets of four peaks (Figure S15). The exchange is dissociative rather than associative, as indicated by the fact that the line widths of (Diso)2Ru-(allylbenzene) are independent of the concentration of the free alkene in the slow exchange regime, as well as by the activation parameters determined from an Eyring plot ( $\Delta H^{\ddagger} = 27.3(14)$ kcal mol<sup>-1</sup>,  $\Delta S^{\ddagger} = 26(4)$  cal mol<sup>-1</sup> K<sup>-1</sup>, Figure S25).

Because rotation is slower than alkene dissociation, the barrier to alkene rotation must be greater than the  $\Delta G^{\ddagger}$  (379) K) =  $17.3 \text{ kcal mol}^{-1}$ . This is substantially greater than the calculated barrier to ethylene rotation in (ap)<sub>2</sub>Ru(CH<sub>2</sub>=CH<sub>2</sub>)  $(\Delta G^{\ddagger} = 12.4 \text{ kcal mol}^{-1})$ , probably because steric interactions between the alkene substituent and the ligand isopropyl groups in the transition state significantly slow rotation compared to the unhindered computational model. The fact that  $\Delta G^{\ddagger}_{diss}$  of the allylbenzene complex is lower than that of the 1-hexyne complex, whose  $\Delta G^{\ddagger}_{rotn}$  of 19.0 kcal mol<sup>-1</sup> at 379 K must be less than its  $\Delta G^{\ddagger}_{
m diss}$ , is consistent with the experimental observation that alkynes bind more strongly to (Diso)2Ru than alkenes. The calculated  $\Delta G^{\circ}$  for dissociation of ethylene from (ap)<sub>2</sub>Ru(CH<sub>2</sub>=CH<sub>2</sub>), 19.9 kcal mol<sup>-1</sup>, is in good agreement with the observed  $\Delta G^{\ddagger}$  for dissociation of alkene from (Diso)<sub>2</sub>Ru(CH<sub>2</sub>=CHCH<sub>2</sub>Ph) extrapolated to 298 K of 19.5 kcal mol<sup>-1</sup>.

Barriers to rotation in alkene and alkyne complexes arise from differences in energy of the two  $d\pi$  orbitals that can potentially interact with the unsaturated ligand. In some cases,

this is due to the geometry of the complex. Examples of this include  $d^{10}$  trigonal planar complexes and  $d^8$  trigonal bipyramidal species (with the alkene equatorial), where  $\sigma^*$  interactions raise the energy of the filled in-plane  $d\pi$  orbital, optimizing backbonding when the alkene (or alkyne) lies in the trigonal plane. In more symmetrical geometries, the barriers to rotation generally reflect the asymmetry in the bonding, for example with the need to compete with nitrosyl showing larger barriers than when the competition is with carbonyl (Table 4).

The geometry of the (Diso)<sub>2</sub>Ru fragment (square pyramidal with apical unsaturated ligand) does not intrinsically foster any differentiation between the relevant  $d\pi$  orbitals, which transform as an E set in  $C_{4v}$  symmetry, nor does it have a strong  $\pi$  acceptor ligand to desymmetrize the  $d\pi$  orbitals as is typical in octahedral complexes with large barriers to alkene or alkyne rotation. Instead, the  $d\pi$  orbitals are distinguished by the  $\pi$  bonding anisotropy of the bis(iminoxolene) fragment, which means that only one  $d\pi$  orbital is strongly engaged in  $\pi$ bonding and so is much lower in energy than the second one. This novel mechanism appears to differentiate the  $d\pi$  orbitals more strongly than a cis carbonyl and is energetically comparable to a cis nitrosyl or to the effect of a trigonal bipyramidal ligand geometry. It is, unsurprisingly, less effective than in  $d^2$  complexes with cis oxo groups<sup>7,37</sup> or bent metallocene geometries,  $^{57}$  where there is only one filled  $d\pi$ orbital.

Stereoselective Alkene Binding by Bis(iminoxolene)-ruthenium. Because both the  $(Diso)_2$ Ru fragment and the 1-alkene are prochiral, there are two possible diastereomers of  $(Diso)_2$ Ru(CH<sub>2</sub>=CHR). For both the allylbenzene and the 1-hexene complex, only one diastereomer can be observed by  $^1$ H NMR spectroscopy (dr > 30:1). The observed species is assigned on the basis of the solid-state structures as the (A,S) diastereomer.  $^{64}$  Since alkene dissociation is fast enough to be observable on the NMR time scale at only moderately elevated temperatures, this selectivity must represent a themodynamic preference.

Although the minor diastereomer cannot be observed experimentally, its properties can be assessed by calculations on the diastereomers of the propene complexes ( $C_6H_4[NR]-O)_2Ru(CH_2=CHMe)$ ). Calculated structures of (diso) $_2Ru(CH_2=CHMe)$ , with the sterically realistic  $R=2,6^{-i}Pr_2C_6H_3$  (Figure 11), clearly show the steric clash between the *N*-aryl substituent and the alkene substituent in the ( $A_1R$ )

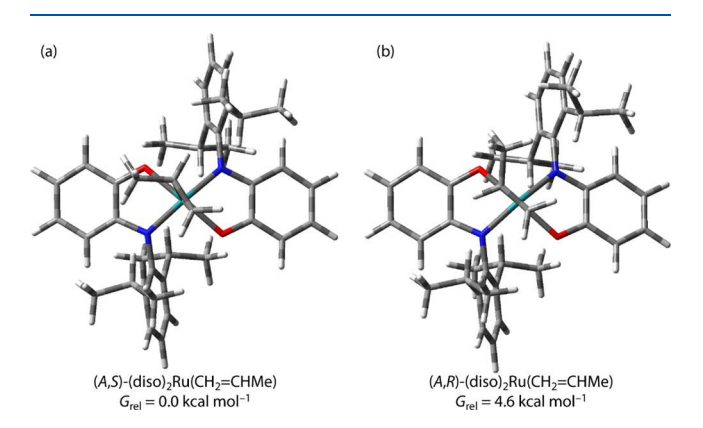


**Figure 11.** Calculated minimum-energy structures of  $(\text{diso})_2\text{Ru}-(\text{CH}_2=\text{CHMe})$ . (a) (A,S) diastereomer  $(G_{\text{rel}}=0)$ . (b) (A,R) diastereomer  $(G_{\text{rel}}=4.6 \text{ kcal mol}^{-1})$ .

diastereomer that is avoided in the (A,S) isomer. This is consistent with the experimental observation that only the latter isomer is observed; computationally the difference in free energy for the two diastereomers of  $(\text{diso})_2\text{Ru}(\text{CH}_2=\text{CHMe})$  is 4.6 kcal  $\text{mol}^{-1}$ . The size of the nitrogen substituent is important energetically, as the compound with R = Ph,  $(\text{ap})_2\text{Ru}(\text{CH}_2=\text{CHMe})$ , is calculated to have the (A,S) isomer only 1.6 kcal  $\text{mol}^{-1}$  more stable than the (A,R) isomer. In the case of the sterically negligible R = H, the diastereomers of  $(\text{hap})_2\text{Ru}(\text{CH}_2=\text{CHMe})$  are essentially isoenergetic, with the (A,R) isomer lower in free energy by 0.1 kcal  $\text{mol}^{-1}$ .

In all of the calculated propene isomers the electronically preferred orientation of the alkene is adopted. There is some variation, with increasing steric strain pushing the alkene toward more positive dihedral angles (e.g.,  $\phi[O1-Ru-C1-C2] = -18.8^{\circ}$  vs  $-1.8^{\circ}$  in (A,S)- and (A,R)-(diso)<sub>2</sub>Ru-(CH<sub>2</sub>=CHMe), respectively), but in all cases the alkene is aligned in the cleft between the iminoxolene ligands, and inclined more toward the O-Ru-O axis. This electronic constraint is key to the high facial selectivity, for without it, both isomers would presumably rotate the alkene to a position with minimal, and similar, steric interactions.

Stereoselective alkene binding to  $C_2$ -symmetric metal centers is uncommon. The closest analogies to the present work are chiral diamine-ligated trigonal planar copper(I)<sup>65,66</sup> or trigonal bipyramidal platinum(II) complexes.<sup>67</sup> In these systems, the coordination geometry imposes an electronic preference for the alkenes to lie in the trigonal plane, and the substituents on the alkene can then experience the dissymmetric environment of the diamine ligands. It is worth noting that these diamine-ligated metal centers do not give high stereoselectivities in binding simple  $\alpha$ -olefins. High (>10:1) stereoselectivity requires additional interactions such as arene-arene contacts from styrenes<sup>65</sup> or metal-oxygen binding from allyl alcohols. 66 The (Diso)<sub>2</sub>Ru fragment has an intrinsically closer approach of the ancillary ligands (90° in the square pyramid vs 120° in the trigonal geometries), and the ortho substituents on the N-aryl groups are directed toward the alkene. The combination of the significant steric profile of the iminoxolene ligands, coupled with the electronic anisotropy of the bis(iminoxolene) fragment to fix the orientation of the C=C bond, allows  $C_2$ -symmetric (Diso)<sub>2</sub>Ru to have a stereoselectivity in binding  $\alpha$ -olefins that is comparable to  $C_1$ -symmetric octahedral complexes.<sup>68</sup>

## CONCLUSIONS

The low-valent iminoxolene complex (Diso)<sub>2</sub>Ru(NCCH<sub>3</sub>)<sub>2</sub> has labile acetonitrile ligands that can be displaced by monosubstituted alkenes or by alkynes to give square pyramidal complexes (Diso)<sub>2</sub>Ru(L). The ruthenium center engages in significant  $\pi$  backbonding to both alkenes and alkynes. The alkyne complexes also show significant donation from the alkyne  $\pi_{\perp}$  orbital to ruthenium, although spectroscopic and structural data indicate that alkyne  $\pi$  donation is slightly outcompeted by iminoxolene—ruthenium  $\pi$  bonding. The nature of the  $\pi$  interactions with the two iminoxolenes is such that one d orbital that is  $\pi$  with respect to the apical position in the square pyramid is strongly engaged with the iminoxolene  $\pi$  orbitals and hence is relatively unavailable for backbonding with the alkene or alkyne. This results in alignment of the C-C multiple bond close to the O-Ru-O axis, but canted toward the cleft between the iminoxolene ligands, in order to maximize backbonding from the other  $d\pi$ 

orbital. In this geometry, the alkyne  $\pi_{\perp}$  orbital mixes with the iminoxolene- $d\pi$  orbitals and gives rise to a favorable four-electron, three-orbital interaction. The alignment is strongly energetically favored, as witnessed by large barriers to rotation of the alkene ( $\Delta G^{\ddagger} > 17.3$  kcal mol<sup>-1</sup> at 379 K for allylbenzene) or alkyne ( $\Delta G^{\ddagger} = 19.0$  kcal mol<sup>-1</sup> at 379 K for 1-hexyne). For alkenes, the electronic anisotropy of the bis(iminoxolene) group that constrains the C=C orientation combines with the positioning of the diisopropylphenyl groups relative to the alkene substituent to give high diastereoselectivity in binding of 1-alkenes, with only one diastereomer observed by <sup>1</sup>H NMR (selectivity of greater than 30:1).

#### EXPERIMENTAL SECTION

General Procedures. Unless otherwise noted, all procedures were carried out in a drybox under a nitrogen atmosphere. Dried solvents were purchased from Acros Organics and were stored in a nitrogenfilled drybox until use. Deuterated solvents were obtained from Cambridge Isotope Laboratories. When dry  $C_6D_6$  was needed, it was dried over sodium and vacuum transferred away from the drying agents and stored in the drybox prior to use. NMR spectra were measured on a Bruker Avance DPX 400 or 500 MHz spectrometer. Chemical shifts for <sup>1</sup>H and <sup>13</sup>C{<sup>1</sup>H} spectra are reported in ppm downfield of TMS, with spectra referenced using the known chemical shifts of the solvent residuals. Infrared spectra were recorded by ATR on a Jasco 6300 FT-IR spectrometer and are reported in wavenumbers. UV-visible-NIR spectra were recorded in 1 cm quartz cells on an Agilent 8453 diode array spectrophotometer or a Jasco V-670 spectrophotometer. Elemental analyses were performed by Robertson Microlit Laboratories (Ledgewood, NJ) or Midwest Microlab (Indianapolis, IN).

cis-(Diso)<sub>2</sub>Ru(NCMe)<sub>2</sub>. In a scintillation vial, 175.5 mg of cis- $(Diso)_2 RuCl_2^{19}$  (0.1885 mmol) and 80.1 mg of  $Cp_2Co$  (0.424 mmol, 2.25 equiv) are dissolved in 5 mL CH<sub>2</sub>Cl<sub>2</sub>. The vial is capped and shaken. The solution immediately turns purple, whereupon 10 mL CH<sub>3</sub>CN is added. The vial is capped and shaken, and allowed to stand at room temperature overnight. The solution is transferred into a round-bottom flask attached to a needle valve, and the solvent is evaporated on the vacuum line. The purple residue is slurried in 4 mL CH<sub>3</sub>CN and filtered on a glass frit. After washing with 3 × 2 mL CH<sub>3</sub>CN, the solid is air-dried for 30 min, and 141.3 mg of cis- $(Diso)_2 Ru(NCMe)_2$  (78%) is isolated. <sup>1</sup>H NMR (C<sub>6</sub>D<sub>6</sub>):  $\delta$  0.94 (d, 6.7 Hz, 6H, CH(CH<sub>3</sub>)Me), 1.03 (d, 6.9 Hz, 6H, CH(CH<sub>3</sub>)Me), 1.05 (s, 6H, CH<sub>3</sub>CN) 1.23 (d, 6.8 Hz, 6H, CH(CH<sub>3</sub>)Me), 1.37 (s, 18H, <sup>t</sup>Bu), 1.40 (s, 18H, <sup>t</sup>Bu), 1.57 (d, 6.8 Hz, 6H, CH(CH<sub>3</sub>)Me), 3.11 (sept, 6.8 Hz, 2H, CHMe<sub>2</sub>), 4.22 (sept, 6.5 Hz, 2H, CHMe<sub>2</sub>), 6.97 (s, 2H, iminoxolene 3- or 5-H), 7.33 (m, 6H, aromatic H).  ${}^{13}C\{{}^{1}H\}$ NMR ( $C_6D_6$ ):  $\delta$  2.77 ( $CH_3CN$ ), 23.82, 24.31, 25.61, 26.47, 26.51, 27.60, 29.05 (C(CH<sub>3</sub>)<sub>3</sub>), 31.38 (C(CH<sub>3</sub>)<sub>3</sub>), 34.33 (C(CH<sub>3</sub>)<sub>3</sub>), 35.21  $(C(CH_3)_3)$ , 111.27, 117.46, 123.16, 123.72, 124.49  $(CH_3CN)$ , 125.39, 136.30, 138.31, 145.04, 146.44, 149.45, 160.24, 173.55 (CO). IR (nujol mull, cm<sup>-1</sup>): 3052 (w), 2275 (m,  $\nu_{C \equiv N}$ ), 1710 (w), 1585 (w), 1526 (m), 1444 (m), 1377 (s), 1357 (m), 1349 (m), 1326 (m), 1302 (m), 1275 (w), 1247 (m), 1232 (s), 1193 (s), 1161 (s), 1110 (m), 1098 (m), 1051 (w), 1040 (w), 1024 (m), 992 (m), 949 (w), 910 (w), 859 (w), 828 (w), 796 (m), 769 (w), 741 (m), 647 (m). UV-vis-NIR (toluene):  $\lambda_{\text{max}} = 1084 \text{ nm}$  ( $\varepsilon = 11,300 \text{ L mol}^{-1}$ cm<sup>-1</sup>), 703 (13500), 558 (11200), 501 (11000), 420 (11400), 352 (7100). The analytical sample contained one acetonitrile of crystallization. Anal. calcd for C<sub>58</sub>H<sub>83</sub>N<sub>5</sub>O<sub>2</sub>Ru: C, 70.84; H, 8.51; N, 7.12. Found: C, 70.71; H, 8.03; N, 7.02.

 $(Diso)_2Ru(CH_2=CHCH_2Ph)$ . In a round-bottom flask, 102.0 mg of cis- $(Diso)_2Ru(NCMe)_2$  (0.1082 mmol) is dissolved in 8 mL dry  $CH_2Cl_2$ . Allylbenzene (720  $\mu$ L, 5.45 mmol, 50 equiv) is added to the purple solution and the flask is swirled to mix. The round-bottom flask is attached to a needle valve. After standing 30 min at room temperature, the solvent is evaporated on the vacuum line. The blueviolet residue is slurried in 2 mL methanol and filtered through a glass

frit. The round-bottom flask is washed with 2 × 2 mL methanol and the washes filtered through the frit. The solid is air-dried for 30 min to yield 75.1 mg of product (70%).  ${}^{1}$ H NMR (C<sub>6</sub>D<sub>6</sub>):  $\delta$  0.75 (d, 6.3 Hz, 3H, CH(CH<sub>3</sub>)Me), 0.81 (d, 7.3 Hz, 3H, CH(CH<sub>3</sub>)Me), 0.92 (d, 7.2 Hz, 3H,  $CH(CH_3)Me$ ), 0.95 (d, 7.0 Hz, 3H,  $CH(CH_3)Me$ ), 1.10 (s, 12H, <sup>t</sup>Bu + CH(CH<sub>3</sub>)Me), 1.14 (s, 9H, <sup>t</sup>Bu), 1.25 (d, 3H, CH(CH<sub>3</sub>)Me), 1.43 (dd, 13.8 Hz, 5.0 Hz, 1H, PhCHH'CH=CH<sub>2</sub>) 1.47 (s, 9H, <sup>t</sup>Bu), 1.52 (d, 7.3 Hz, 3H, CH(CH<sub>3</sub>)Me), 1.57 (s, 12H, <sup>t</sup>Bu + CH(CH<sub>3</sub>)Me), 1.75 (dd, 9.2, 3.2 Hz, 1H, trans-PhCH<sub>2</sub>CH=CHH'), 1.92 (sept, 7.0 Hz, 1H, CHMe<sub>2</sub>), 1.99 (sept, 6.8 Hz, 1H, CHMe<sub>2</sub>), 2.57 (sept, 6.7 Hz, 1H, CHMe<sub>2</sub>), 2.71 (dd, 3.9, 13.9 Hz, 1H, PhCHH'CH=CH<sub>2</sub>), 3.23 (sept, 6.5 Hz, 1H, CHMe<sub>2</sub>), 5.08 (dd, 12.6, 3.3 Hz, 1H, cis-PhCH<sub>2</sub>CH=CHH'), 5.61 (m, 1H, PhCH<sub>2</sub>CH=CH<sub>2</sub>), 6.80 (d, 1.9 Hz, 1H, iminoxolene 3- or 5-H), 6.84 (d, 2.0 Hz, 1H, iminoxolene 3- or 5-H), 6.99 (m, 1H, p-Ph), 7.05-7.14 (m, 6H, o,m-Ph + Ar 4-H), 7.30-7.40 (m, 5H, Ar 3,5-H + iminoxolene 3- or 5-H, 7.45 (d, 2.0 Hz, 1H, iminoxolene 3- or 5-H).  $^{13}C\{^{1}H\}$  NMR  $(C_6D_6)$ :  $\delta$  23.66 (2C, CH(CH<sub>3</sub>)Me), 23.74 (CH(CH<sub>3</sub>)Me), 24.72 (CH(CH<sub>3</sub>)Me), 25.37 (CH(CH<sub>3</sub>)Me), 25.61 (CH(CH<sub>3</sub>)Me), 25.66 (CH(CH<sub>3</sub>)Me), 25.95 (CH(CH<sub>3</sub>)Me), 28.75 (CHMe<sub>2</sub>), 28.87 (CHMe<sub>2</sub>), 29.15 (CHMe<sub>2</sub>), 29.34 (CHMe<sub>2</sub>), 30.08  $(C(CH_3)_3)$ , 30.64  $(C(CH_3)_3)$ , 30.95  $(C(CH_3)_3)$ , 31.10  $(C(CH_3)_3)$ , 34.19  $(C(CH_3)_3)$ , 34.23  $(C(CH_3)_3)$ , 35.16  $(C(CH_3)_3)$ , 35.38  $(C(CH_3)_3)$ , 37.66 (PhCH<sub>2</sub>), 59.66 (H<sub>2</sub>C=CH), 73.14 (H<sub>2</sub>C=CH), 112.00, 112.50, 121.11, 121.43, 122.89, 124.33, 124.41, 126.06, 128.34, 128.42, 137.85, 138.21, 138.31, 138.78, 141.03, 141.31, 141.66, 142.45, 142.89 149.72, 150.02, 157.67, 158.87, 170.65 (CO), 171.44 (CO). IR (nujol mull, cm<sup>-1</sup>): 3060 (w), 1541 (w), 1528 (w), 1378 (s), 1356 (w), 1312 (w), 1299 (w), 1247 (m), 1229 (m), 1203 (m), 1154 (m), 1102 (w), 1031 (w), 996 (w), 922 (w), 865 (m), 821 (w), 803 (w), 781 (w), 746 (w), 737 (w), 698 (w), 663 (w), 654 (w). UV-vis (toluene):  $\lambda_{\text{max}} = 700 \text{ nm } (\varepsilon = 14,500 \text{ L mol}^{-1} \text{ cm}^{-1}), 573$ (9400), 494 (10400), 414 (9700). Anal. calcd for  $C_{61}H_{84}N_2O_2Ru$ : C, 74.88; H, 8.65; N, 2.86. Found: C, 74.46; H, 8.01; N, 2.65.

(Diso)<sub>2</sub>Ru(CH<sub>2</sub>=CHBu). The 1-hexene complex is prepared by the method used for the allylbenzene derivative using 51.9 mg of cis- $(Diso)_2Ru(NCMe)_2$  (0.0551 mmol) and 350  $\mu L$  of 1-hexene (2.81 mmol, 50 equiv) and yields 32.0 mg of (Diso)<sub>2</sub>Ru(1-hexene) (61%). <sup>1</sup>H NMR ( $C_6D_6$ ):  $\delta$  0.14 (m, 1H,  $CH_3(CH_2)_2CHH'CH=CH_2$ ) 0.69 (t, 7.1 Hz, 3H,  $CH_3(CH_2)_3CH=CH_2$ ), 0.74 (d, 6.8 Hz, 3H, CH(CH<sub>3</sub>)Me), 0.79 (d, 6.9 Hz, 3H, CH(CH<sub>3</sub>)Me), 0.93 (d, 6.6 Hz, 3H,  $CH(CH_3)Me$ ), 0.95 (d, 6.7 Hz, 3H,  $CH(CH_3)Me$ ), 1.11 (s, 9H, <sup>t</sup>Bu), 1.12 (s, 9H, <sup>t</sup>Bu), 1.18 (d, 6.8 Hz, 3H, CH(CH<sub>3</sub>)Me), 1.27 (d, 7.2 Hz, 3H, CH(CH<sub>3</sub>)Me), 1.48 (s, 9H, <sup>t</sup>Bu), 1.52 (s, 9H, <sup>t</sup>Bu), 1.54 (d, 6.8 Hz, 3H, CH(CH<sub>3</sub>)Me), 1.59 (d, 6.6 Hz, 3H, CH(CH<sub>3</sub>)Me), 1.83 (dd, 9.6, 3.2 Hz, 1H, trans- $CH_3(CH_2)_3CH=CH'H)$ , 1.92 (sept, 6.9 Hz, 1H,  $CHMe_2$ ), 1.99 (sept, 7.1 Hz, 1H, CHMe<sub>2</sub>), 2.61 (sept, 6.6 Hz, 1H, CHMe<sub>2</sub>), 3.06 (sept, 7.0 Hz, 1H, CHMe<sub>2</sub>), 4.87 (dd, 13.2, 3.4 Hz, 1H, cis- $CH_3(CH_2)_3CH = CHH'$ ), 5.39 (m, 1H,  $CH_3(CH_2)_3CH = CH_2$ ), 6.80 (d, 2.4 Hz, 1H, iminoxolene 3- or 5-H), 6.83 (d, 2.0 Hz, 1H, iminoxolene 3- or 5-H), 7.07-7.11 (m, 2H, Ar 3- or 5-H, + Ar 4-H), 7.29-7.37 (m, 4H, Ar 3- and 5-H + Ar 3- or 5-H + Ar 4-H), 7.41 (d, 2.2 Hz, 1H, iminoxolene 3- or 5-H), 7.43 (d, 2.2 Hz, 1H, iminoxolene 3- or 5-H). (Five of the protons from the bound hexene are multiplets that were obscured by the more intense signals from 1 to 2 ppm.) <sup>13</sup>C{<sup>1</sup>H} NMR ( $C_6D_6$ ):  $\delta$  14.29 ( $CH_3(CH_2)_3CH=CH_2$ ), 22.76 (CH<sub>3</sub>CH<sub>2</sub>(CH<sub>2</sub>)<sub>2</sub>CH=CH<sub>2</sub>), 24.39 (CH(CH<sub>3</sub>)Me), 24.44 (CH-(CH<sub>3</sub>)Me), 24.50 (CH(CH<sub>3</sub>)Me), 25.27 (CH(CH<sub>3</sub>)Me), 26.08 (CH(CH<sub>3</sub>)Me), 26.33 (CH(CH<sub>3</sub>)Me), 26.56 (CH(CH<sub>3</sub>)Me), 26.66  $(CH(CH_3)Me)$ , 29.12  $(CHMe_2)$ , 29.56  $(CHMe_2)$ , 29.86  $(CHMe_2)$ , 30.03 (CHMe<sub>2</sub>), 30.79 (C(CH<sub>3</sub>)<sub>3</sub>), 30.94 $(CH_3CH_2CH_2CH_2CH_2CH_2)$ , 31.24  $(C(CH_3)_3)$ , 31.73  $(C(CH_3)_3)$ , 31.82 ( $C(CH_3)_3$ ), 33.93 ( $CH_3(CH_2)_2CH_2CH=CH_2$ ), 34.89 (C(CH3)3), 34.98 (C(CH3)3), 35.92 (C(CH3)3), 36.06 (C(CH3)3), 61.44 (BuCH=CH<sub>2</sub>), 75.83 (BuCH=CH<sub>2</sub>), 112.77, 113.05, 121.71, 121.89, 123.54, 123.77, 125.08 (2C), 138.32, 138.66, 139.04, 139.47, 141.64, 141.97, 143.16, 143.58, 150.56, 150.89, 158.51, 159.57, 171.07 (CO), 172.14 (CO). Two resonances

are obscured by the  $C_6D_6$  solvent peak. IR (nujol mull, cm $^{-1}$ ): 3056 (w), 1576 (w), 1542 (m), 1373 (s), 1356 (s), 1311 (m), 1305 (m), 1221 (s), 1198 (s), 1159 (s), 1097 (w), 1046 (w), 1030 (w), 990 (w), 951 (w), 934 (w), 911 (w), 883 (w), 861 (m), 821 (w), 787 (w), 782 (w), 765 (w), 742 (w), 714 (w). UV—vis (toluene):  $\lambda_{\rm max}=698$  nm ( $\varepsilon=13400$  L mol $^{-1}$  cm $^{-1}$ ), 581 (9000), 492 (9500), 410 (9500). Anal. calcd for  $C_{58}H_{86}N_2O_2Ru$ : C, 73.76; H, 9.18; N, 2.97. Found: C, 70.47; H, 8.73; N, 2.71.

(Diso)<sub>2</sub>Ru(HC≡CBu). The 1-hexyne complex is prepared by the method used for the allylbenzene derivative using 65.1 mg of cis-(Diso)2Ru(NCMe)<sub>2</sub> (0.0691 mmol) and 73.0  $\mu$ L of 1-hexyne (2.81 mmol, 9 equiv) and yields 36.1 mg of (Diso)<sub>2</sub>Ru(1-hexyne) (58%). <sup>1</sup>H NMR (C<sub>6</sub>D<sub>6</sub>):  $\delta$  0.69 (t, 7.3 Hz, 3H, HC≡CCH<sub>2</sub>CH<sub>2</sub>CH<sub>2</sub>CH<sub>3</sub>) 0.84 (d, 6.3 Hz, 3H, CH(CH<sub>3</sub>)Me), 0.85 (d, 6.1 Hz, 3H, CH(CH<sub>3</sub>)Me), 0.91 (d, 6.3 Hz, 3H, CH(CH<sub>3</sub>)Me), 1.01 (d, 6.3 Hz, 3H,  $CH(CH_3)Me$ ), 1.06 (d, 6.0 Hz, 3H,  $CH(CH_3)Me$ ), 1.09 (d, 6.6 Hz, 3H, CH(CH<sub>3</sub>)Me), 1.11 (s, 9H,  ${}^{t}Bu$ ), 1.14 (m, 2H, HC= CCH<sub>2</sub>CH<sub>2</sub>CH<sub>2</sub>CH<sub>3</sub>), 1.16 (s, 9H, <sup>t</sup>Bu), 1.28 (m, 2H, HC≡ CCH<sub>2</sub>CH<sub>2</sub>CH<sub>2</sub>CH<sub>3</sub>), 1.36 (d, 6.6 Hz, 3H, CH(CH<sub>3</sub>)Me), 1.42 (d, 6.6 Hz, 3H, CH(CH<sub>3</sub>)Me), 1.51 (s, 9H, <sup>t</sup>Bu), 1.53 (s, 9H, <sup>t</sup>Bu), 2.21 (sept, 6.6 Hz, 1H, CHMe<sub>2</sub>), 2.32 (sept, 6.2 Hz, 1H, CHMe<sub>2</sub>), 2.42 (sept, 6.9 Hz, 1H, CHMe<sub>2</sub>), 2.69 (sept, 6.6 Hz, 1H, CHMe<sub>2</sub>), 2.92 (dt, 17.1, 7.1 Hz, 1H, HC $\equiv$ CCHH'CH<sub>2</sub>CH<sub>2</sub>CH<sub>3</sub>), 3.16 (dt, 17.1, 6.7 Hz, 1H, HC≡CCHH'CH<sub>2</sub>CH<sub>2</sub>CH<sub>3</sub>), 6.58 (d, 2.2 Hz, 1H, iminoxolene 3- or 5-H), 6.59 (d, 2.3 Hz, 1H, iminoxolene 3- or 5-H), 7.12 (dd, 8.1, 1.2 Hz, 1H, Ar 3- or 5-H), 7.18 (dd, 7.8, 1.3 Hz, 1H, Ar 3- or 5-H), 7.24 (dd, 7.9, 1.1 Hz, 1H, Ar 3- or 5-H), 7.30-7.39 (m, 5H, 2 Ar 4-H + Ar 3- or 5-H, + iminoxolene 3- and 5-H), 7.73 (s, 1H,  $HC \equiv CCH_2CH_2CH_2CH_3$ ). <sup>13</sup> $C\{^1H\}$  NMR  $(C_6D_6)$ :  $\delta$  13.40  $(HC \equiv CCH_2CH_2CH_2CH_3)$ , 21.76  $(HC \equiv CCH_2CH_2CH_2CH_3)$ , 23.14 (CH(CH<sub>3</sub>)Me), 23.89 (CH(CH<sub>3</sub>)Me), 24.52 (CH(CH<sub>3</sub>)Me), 25.02 (CH(CH<sub>3</sub>)Me), 25.32 (CH(CH<sub>3</sub>)Me), 25.41 (CH(CH<sub>3</sub>)Me), 25.44 (CH(CH<sub>3</sub>)Me), 25.83 (HC≡CCH<sub>2</sub>CH<sub>2</sub>CH<sub>2</sub>CH<sub>3</sub>), 26.36 (CH(CH<sub>3</sub>)Me), 27.69 (CHMe<sub>2</sub>), 27.84 (CHMe<sub>2</sub>), 28.70 (CHMe<sub>2</sub>), 28.73 (CHMe<sub>2</sub>), 30.35 (C(CH<sub>3</sub>)<sub>3</sub>), 30.99 (C(CH<sub>3</sub>)<sub>3</sub>), 31.54 (C- $(CH_3)_3$ , 31.60  $(C(CH_3)_3)$ , 32.81  $(HC \equiv CCH_2CH_2CH_2CH_3)$ , 34.18  $(C(CH_3)_3)$ , 34.25  $(C(CH_3)_3)$ , 35.31  $(C(CH_3)_3)$ , 35.42  $(C(CH_3)_3)$ , 111.87, 112.07, 116.17 (HC $\equiv$ CCH<sub>2</sub>CH<sub>2</sub>CH<sub>2</sub>CH<sub>3</sub>), 120.22, 121.09, 122.89, 123.46, 124.96, 125.15, 136.70, 137.02, 137.86, 138.10, 140.04 (HC≡CCH<sub>2</sub>CH<sub>2</sub>CH<sub>2</sub>CH<sub>3</sub>), 142.77, 143.00, 143.02, 143.24, 148.63, 149.29, 153.91, 154.93, 166.02 (CO), 166.16 (CO). IR (nujol mull, cm<sup>-1</sup>): 1577 (w), 1543 (w), 1379 (s), 1371 (m), 1311 (w), 1294 (w), 1255 (m), 1224 (m), 1221 (m), 1201 (m), 1160 (m), 1097 (w), 1053 (w), 1029 (w), 997 (w), 933 (w), 918 (w), 904 (w), 867 (m), 829 (w), 798 (m), 767 (w), 729 (w), 721 (m), 696 (w). 667 (w). UV-vis (toluene):  $\lambda_{\text{max}} = 593 \text{ nm} \ (\varepsilon = 18,400 \text{ L mol}^{-1} \text{ cm}^{-1})$ , 460 (10,200), 402 (sh, 10,300). Anal. calcd for C<sub>58</sub>H<sub>84</sub>N<sub>2</sub>O<sub>2</sub>Ru: C, 73.92; H, 8.98; N, 2.97. Found: C, 73.55; H, 8.74; N, 2.92.

(Diso)<sub>2</sub>Ru(EtC≡CEt) is generated in situ by treating 16.2 mg cis- $(Diso)_2 Ru(NCCH_3)_2$  (0.0172 mmol) with 5.0  $\mu$ L 3-hexyne (0.0440 mmol, 2.6 equiv) in 0.6 mL CD<sub>2</sub>Cl<sub>2</sub>. The blue-violet solution is analyzed by <sup>1</sup>H and <sup>13</sup>C{<sup>1</sup>H} NMR spectroscopy. <sup>1</sup>H NMR  $(CD_2Cl_2)$ :  $\delta$  0.60 (d, 6.8 Hz, 6H,  $CH(CH_3)Me$ ), 0.74 (d, 6.7 Hz, 6H, CH(CH<sub>3</sub>)Me), 0.77 (d, 6.7 Hz, 6H, CH(CH<sub>3</sub>)Me), 0.99 (t, 7.4 Hz, 6H, CH<sub>2</sub>CH<sub>3</sub>), 1.06 (s, 18H, <sup>t</sup>Bu), 1.18 (s, 18H, <sup>t</sup>Bu), 1.30 (d, 6.8 Hz, 6H, CH(CH<sub>3</sub>)Me), 2.78 (dq, 16.3, 7.6 Hz, 2H, CHH'CH<sub>3</sub>), 3.11 (dq, 16.4, 7.5 Hz, 2H, CHH'CH<sub>3</sub>), 6.14 (d, 2.0 Hz, 2H, iminoxolene 3- or 5-H), 7.02 (d, 2.0 Hz, 2H, iminoxolene 3- or 5-H), 7.17 (d, 7.5 Hz, 2H, Ar 3- or 5-H), 7.24 (d, 7.1 Hz, 2H, Ar 3- or 5-H), 7.35 (t, 7.7 Hz, 2H, Ar 4-H).  $^{13}C\{^{1}H\}$  NMR (CD<sub>2</sub>Cl<sub>2</sub>):  $\delta$  15.57 (CH<sub>2</sub>CH<sub>3</sub>), 20.85 (CH(CH<sub>3</sub>)Me), 23.29 (CH(CH<sub>3</sub>)Me), 24.96 (CH(CH<sub>3</sub>)Me), 25.14 (CH(CH<sub>3</sub>)Me), 25.29 (CH<sub>2</sub>CH<sub>3</sub>), 27.83 (CHMe<sub>2</sub>), 28.53  $(CHMe_2)$ , 31.15  $(C(CH_3)_3)$ , 31.59  $(C(CH_3)_3)$ , 34.28  $(C(CH_3)_3)$ , 35.32 (C(CH<sub>3</sub>)<sub>3</sub>), 112.37, 120.67, 122.87, 125.16, 127.80, 136.13,  $137.18, 139.68 \ (C \equiv C), 143.28, 143.55, 149.24, 153.89, 164.76 \ (CO).$ 

**Variable-Temperature NMR Spectroscopy.** High-temperature NMR spectra were acquired using toluene- $d_8$  solutions on a Bruker AVANCE DPX-400 MHz NMR spectrometer for (Diso)<sub>2</sub>Ru-(CH<sub>2</sub>=CHCH<sub>2</sub>Ph) and a Bruker AVANCE DPX-500 MHz NMR spectrometer for cis-(Diso)<sub>2</sub>Ru(NCCH<sub>3</sub>)<sub>2</sub> and (Diso)<sub>2</sub>Ru(1-hexyne),

with probe temperatures calibrated using the peak separation in ethylene glycol. <sup>69</sup> The bound and free acetonitrile resonances of *cis*-(Diso)<sub>2</sub>Ru(NCCH<sub>3</sub>)<sub>2</sub>, the *tert*-butyl protons and the bound and free H<sub>2</sub>C=CHR of the alkene of (Diso)<sub>2</sub>Ru(CH<sub>2</sub>=CHCH<sub>2</sub>Ph), and the *tert*-butyl protons of (Diso)<sub>2</sub>Ru(1-hexyne) were simulated using the dynamic NMR simulation routine in Topspin 3.6. For temperatures above the coalescence point, chemical shifts of the *tert*-butyl peaks were estimated by linear extrapolation of the temperature-dependent shifts, and the extrapolated difference in chemical shifts was treated as fixed in the simulation.

**X-ray Crystallography.** Crystals of  $(Diso)_2Ru(NCMe)_2 \cdot 2CH_3CN$  were grown by liquid diffusion of acetonitrile into a dichloromethane solution of the complex. Crystals of  $(Diso)_2Ru(CH_2=CHCH_2Ph)$ ,  $(Diso)_2Ru(CH_2=CHBu) \cdot CH_2Cl_2$ , and  $(Diso)_2Ru(EtC \equiv CEt) \cdot 0.5CH_2Cl_2$  were grown from liquid diffusion of methanol into dichloromethane solutions of the complexes. Crystals were placed in inert oil before being transferred to the cold  $N_2$  stream of the diffractometer. The data were reduced, correcting for absorption, using the program SADABS.

In (Diso)<sub>2</sub>Ru(CH<sub>2</sub>=CHBu)·CH<sub>2</sub>Cl<sub>2</sub>, the 1-hexene is disordered about the crystallographic 2-fold axis. Because the 1- and 2-carbons are each close to the other's symmetry equivalent, they were refined with their thermal parameters constrained to be equivalent to each other. The dichloromethane solvent was partially occupied and was arbitrarily assigned an occupancy of 50%. The bound allylbenzene in (Diso)<sub>2</sub>Ru(CH<sub>2</sub>=CHCH<sub>2</sub>Ph) was disordered about the crystallographic 2-fold analogously to the 1-hexene in the hexene complex. Additionally, the tert-butyl group centered at C18, C23-C25 of the diisopropylphenyl group, both isopropyl groups, and the phenyl ring of the allylbenzene were all modeled as occupying two different orientations. In each case, the corresponding atoms in the two orientations were constrained to have the same thermal parameters, with the occupancies allowed to refine. The phenyl groups were refined as rigid groups using the AFIX 66 instruction and their thermal parameters were restrained to be similar using the SIMU instruction. In the structure of (Diso)₂Ru(EtC≡CEt)·0.5CH₂Cl₂, there were two independent ruthenium complexes in the asymmetric unit. In one of them (Ru2), there was a small amount of wholemolecule disorder where there was a small amount of the species with the ruthenium and hexyne on the other side of the bis(iminoxolene) unit. Only the Ru of this orientation was modeled; its thermal parameters were constrained to be equal to those of Ru2 and its occupancy refined to 4.97(4)%. One tert-butyl group (centered on C58) was disordered in two different orientations; opposing methyl groups were constrained to have equal thermal parameters and the occupancies allowed to refine. The lattice dichloromethane had one chlorine disordered in two different locations.

All nonhydrogen atoms were refined anisotropically. Hydrogen atoms in *cis*-(Diso)<sub>2</sub>Ru(NCMe)<sub>2</sub>·2CH<sub>3</sub>CN were found on difference Fourier maps and refined isotropically, while lattice solvent hydrogen atoms were placed in calculated positions. Hydrogen atoms in the remaining three structures were placed in calculated positions with their thermal parameters tied to the isotropic thermal parameters of the atoms to which they are bonded (1.5× for methyl, 1.2× for all others). Calculations used SHELXTL (Bruker AXS),<sup>70</sup> with scattering factors and anomalous dispersion terms taken from the literature.<sup>71</sup>

Computational Methods. Geometry optimizations were performed on simplified structures in which *tert*-butyl groups were replaced by hydrogen; the nitrogen substituent in the iminoxolene was either hydrogen (hap ligand), phenyl (ap), or 2,6-diisopropylphenyl (diso). Hydrogen cyanide was used in place of acetonitrile in the relevant compounds. Calculations used density functional theory (B3LYP, SDD basis set for Ru, 6-31G\* basis set for all other atoms) as implemented in the Gaussian16 suite of programs.<sup>72</sup> The optimized geometries for stable species were confirmed as minima, and of transition states as first-order saddle points, by calculation of vibrational frequencies. Plots of calculated Kohn—Sham orbitals were generated using Gaussview (v. 6.0.16) with an isovalue of 0.04.

#### ASSOCIATED CONTENT

# **Supporting Information**

The Supporting Information is available free of charge at https://pubs.acs.org/doi/10.1021/acs.organomet.4c00259.

Summary of crystal data, NMR spectra, infrared spectra, UV-visible spectra, summaries of spectroscopic and structural data on known ruthenium alkene and alkyne complexes, and calculated structures, energies, and MOS values (PDF)

Cartesian coordinates of optimized structures by DFT (XYZ)

#### **Accession Codes**

CCDC 2359508–2359511 contain the supplementary crystallographic data for this paper. These data can be obtained free of charge via <a href="www.ccdc.cam.ac.uk/data\_request/cif">www.ccdc.cam.ac.uk/data\_request/cif</a>, or by emailing <a href="data\_request@ccdc.cam.ac.uk">data\_request/cif</a>, or by contacting the Cambridge Crystallographic Data Centre, 12 Union Road, Cambridge CB2 1EZ, UK; fax: + 44 1223 336033.

### AUTHOR INFORMATION

#### **Corresponding Author**

Seth N. Brown — Department of Chemistry and Biochemistry, University of Notre Dame, Notre Dame, Indiana 46556-5670, United States; orcid.org/0000-0001-8414-2396; Email: Seth.N.Brown.114@nd.edu

#### **Author**

Patricia Rose H. Ayson – Department of Chemistry and Biochemistry, University of Notre Dame, Notre Dame, Indiana 46556-5670, United States

Complete contact information is available at: https://pubs.acs.org/10.1021/acs.organomet.4c00259

#### Notes

The authors declare no competing financial interest.

# ACKNOWLEDGMENTS

This work was supported by the US National Science Foundation (CHE-1955933 and CHE-2400019). We thank Dr. Allen G. Oliver for his assistance with X-ray crystallography, and the NSF for their support of the acquisition of the diffractometer used for the structure of (Diso)₂Ru(EtC≡ CEt)·0.5 CH₂Cl₂ (MRI award CHE-2214606). We thank Dr. Evgenii Kovrigin for his help with the NMR experiments.

#### REFERENCES

- (1) Jerabek, P.; Schwerdtfeger, P.; Frenking, G. Dative and Electron-Sharing Bonding in Transition Metal Compounds. *J. Comput. Chem.* **2019**, *40*, 247–264.
- (2) Templeton, J. L. 4-Electron Alkyne Ligands in Molybdenum(II) and Tungsten(II) Complexes. *Adv. Organomet. Chem.* **1989**, 29, 1–100.
- (3) Górski, M.; Kochel, A.; Szymańska-Buzar, T. A new synthetic route to pentacarbonylalkene complexes of tungsten(0): X-ray crystal structure of  $[W(CO)_5(\eta^2-C_2H_4)]$ . Inorg. Chem. Commun. **2006**, 9, 136–138
- (4) Pidun, U.; Frenking, G. Complexes of Transition Metals in High and Low Oxidation States with Side-On-Bonded  $\pi$ -Ligands. *Organometallics* **1995**, *14*, 5325–5336.
- (5) Bodner, G. S.; Peng, T.-S.; Arif, A. M.; Gladysz, J. A. Synthesis, Structure, and Reactivity of Chiral Rhenium Alkene Complexes of the Formula  $[(\eta^{S}-C_{S}H_{S})Re(NO)(PPh_{3})(H_{2}C=CHR)]^{+}X^{-}$ . Organometallics 1990, 9, 1191–1205.

- (6) Friedman, L. A.; Meiere, S. H.; Brooks, B. C.; Harman, W. D. Ethylene Rotation in Chiral Octahedral Rhenium(I) Complexes. *Organometallics* **2001**, *20*, 1699–1702.
- (7) Su, F.-M.; Cooper, C.; Geib, S. J.; Rheingold, A. L.; Mayer, J. M. Synthesis and Characterization of High-Valent Oxo–Olefin and Oxo–Carbonyl Complexes. Crystal and Molecular Structure of W(O)Cl<sub>2</sub>(CH<sub>2</sub>=CH<sub>2</sub>)(PMePh<sub>2</sub>)<sub>2</sub>. J. Am. Chem. Soc. **1986**, 108, 3545–3547.
- (8) Faller, J. W. Stereochemical Nonrigidity of Organometallic Complexes. In *Encyclopedia of Inorganic Chemistry*; King, R. B., ed.; John Wiley & Sons: New York, 1994; pp 3914–3933.
- (9) Sanaú, M.; Peng, T.-S.; Arif, A. M.; Gladysz, J. A. Crystal structures of diastereomeric styrene complexes of the chiral rhenium fragment  $[(\eta^5-C_5H_5)Re(NO)(PPh_3)]^+$ : effect of ligating enantioface upon bonding and conformation. *J. Organomet. Chem.* **1995**, 503, 235–241.
- (10) Peng, T.-S.; Arif, A. M.; Gladysz, J. A. Thermodynamic Enantioface-Binding Selectivities of Monosubstituted Alkenes to a Highly Discriminating Chiral Transition-Metal *Lewis* Acid; Equilibration of Diastereoisomeric (Cyclopentadienyl)(alkene)(nitrosyl)(triphenylphosphine)rhenium Complexes ([Re( $\eta^5$ -C<sub>5</sub>H<sub>5</sub>)-(CH<sub>2</sub>=CHR)(NO)(PPh<sub>3</sub>)]+BF<sub>4</sub>-). *Helv. Chim. Acta* **1992**, 75, 442–456.
- (11) Peng, T.-S.; Winter, C. H.; Gladysz, J. A. Generation and Reactivity of Substitution-Labile Dichloromethane and Chlorobenzene Adducts of the Chiral *Pentamethyl*cyclopentadienyl Rhenium Lewis Acid  $[(\eta^5-C_5Me_5)Re(NO)(PPh_3)]^+$ . *Inorg. Chem.* **1994**, 33, 2534–2542.
- (12) Whitesell, J. K. C<sub>2</sub> Symmetry and Asymmetric Induction. *Chem. Rev.* **1989**, *89*, 1581–1590.
- (13) Gianino, J.; Brown, S. N. Highly covalent metal-ligand  $\pi$  bonding in chelated bis- and tris(iminoxolene) complexes of osmium and ruthenium. *Dalton Trans.* **2020**, *49*, 7015–7027.
- (14) Do, T. H.; Brown, S. N. Mono- and Bis(iminoxolene)iridium Complexes: Synthesis and Covalency in  $\pi$  Bonding. *Inorg. Chem.* **2022**, *61*, 5547–5562.
- (15) Cipressi, J.; Brown, S. N. Octahedral to trigonal prismatic distortion driven by subjacent orbital  $\pi$  antibonding interactions and modulated by ligand redox noninnocence. *Chem. Commun.* **2014**, *50*, 7956–7959.
- (16) Gianino, J.; Erickson, A. N.; Markovitz, S. J.; Brown, S. N. High-valent osmium iminoxolene complexes. *Dalton Trans.* **2020**, *49*, 8504–8515.
- (17) Carbonel, H.; Mikulski, T. D.; Nugraha, K.; Johnston, J.; Wang, Y.; Brown, S. N. Optically active bis(aminophenols) and their metal complexes. *Dalton Trans.* **2023**, *52*, 13290–13303.
- (18) Erickson, A. N.; Gianino, J.; Markovitz, S. J.; Brown, S. N. Amphiphilicity in Oxygen Atom Transfer Reactions of Oxobis-(iminoxolene)osmium Complexes. *Inorg. Chem.* **2021**, *60*, 4004–4014
- (19) Ayson, P. R. H.; Brown, S. N. Slip to  $\pi$  Ru: structural distortions due to metal-iminoxolene  $\pi$  bonding. *Chem. Commun.* **2023**, *59*, 9618–9621.
- (20) Brown, S. N. Metrical Oxidation States of 2-Amidophenoxide and Catecholate Ligands: Structural Signatures of Metal–Ligand  $\pi$  Bonding in Potentially Noninnocent Ligands. *Inorg. Chem.* **2012**, *51*, 1251–1260.
- (21) Do, T. H.; Haungs, D. A.; Chin, W. Y.; Jerit, J. T.; VanderZwaag, A.; Brown, S. N. Modulation of Isomerization and Ligand Exchange Rates by  $\pi$  Bonding in Bis(iminoxolene)iridium Pyridine Complexes. *Inorg. Chem.* **2023**, *62*, 11718–11730.
- (22) Das, D.; Mondal, T. K.; Chowdhury, A. D.; Weisser, F.; Schweinfurth, D.; Sarkar, B.; Mobin, S. M.; Urbanos, F. A.; Jiménez-Aparicio, R.; Lahiri, G. K. Valence and spin situations in isomeric  $[(bpy)Ru(Q')_2]^n$  (Q'=3,5-di-tert-butyl-N-aryl-1,2-benzoquinonemonoimine). An experimental and DFT analysis. *Dalton Trans.* **2011**, *40*, 8377–8390.
- (23) Pace, E. L.; Noe, L. J. Infrared Spectra of Acetonitrile and Acetonitrile-*d*<sub>3</sub>. *J. Chem. Phys.* **1968**, *49*, 5317–5325.

- (24) Rüba, E.; Simanko, W.; Mauthner, K.; Soldouzi, K. M.; Slugove, C.; Mereiter, K.; Schmid, R.; Kirchner, K.  $[RuCp(PR_3)(CH_3CN)_2]$ -PF<sub>6</sub> (R = Ph, Me, Cy). Convenient Precursors for Mixed Ruthenium(II) and Ruthenium(IV) Half-Sandwich Complexes. Organometallics **1999**, *18*, 3843–3850.
- (25) Hasegawa, T.; Lau, T. C.; Taube, H.; Schaefer, W. P. Electronic Effects of Bis(acetylacetone) in Ruthenium(II) and Ruthenium(III) Complexes. *Inorg. Chem.* **1991**, *30*, 2921–2928.
- (26) Lai, Y.-H.; Chen, Y.-L.; Chi, Y.; Liu, C.-S.; Carty, A. J.; Peng, S.-M.; Lee, G.-H. Deposition of Ru and RuO<sub>2</sub> thin films employing dicarbonyl bis-diketonate ruthenium complexes as CVD source reagents. *J. Mater. Chem.* **2003**, *13*, 1999–2006.
- (27) Bruce, M. I. Organometallic Chemistry of Vinylidene and Related Unsaturated Carbenes. *Chem. Rev.* **1991**, *91*, 197–257.
- (28) Puerta, M. C.; Valerga, P. Ruthenium and osmium vinylidene complexes and some related compounds. *Coord. Chem. Rev.* **1999**, 193–195, 977–1025.
- (29) Scott, A. P.; Radom, L. Harmonic Vibrational Frequencies: An Evaluation of Hartree-Fock, Møller-Plesset, Quadratic Configuration Interaction, Density Functional Theory, and Semiemprical Scale Factors. *J. Phys. Chem.* **1996**, *100*, 16502–16513.
- (30) Addison, A. W.; Rao, T. N.; Reedijk, J.; van Rijn, J.; Verschoor, G. C. Synthesis, Structure, and Spectroscopic Properties of Copper(II) Compounds containing Nitrogen—Sulphur Donor Ligands; the Crystal and Molecular Structure of Aqua[1,7-bis(N-methylbenzimidazol-2'-yl)-2,6-dithiaheptane]copper(II) Perchlorate. *J. Chem. Soc., Dalton Trans.* 1984, 1349—1356.
- (31) Koelle, U.; Kang, B.-S.; Spaniol, T. P.; Englert, U. Reactions of  $[Cp*Ru(OMe)]_2$ . 9. Olefin Activation and Formation of Allyl Complexes. Molecular Structure of  $Cp*Ru(\eta^3-C_3H_5)(\eta^2-CH_3=CHCH_3)$ . Organometallics 1992, 11, 249–254.
- (32) Capelle, B.; Dartiguenave, M.; Dartiguenave, Y.; Beauchamp, A. L. (Trimethylphosphine)cobalt(I) Complexes. 2. Reactivity with Diphenylacetylene: Chemical and Structural Evidence for Alkyne Ligand as Variable-Electron Donor in  $[Co(MeCN)(C_2Ph_2)(PMe_3)_3]$ BPh<sub>4</sub> and  $[Co(C_2Ph_2)(PMe_3)_3]$ BPh<sub>4</sub>. J. Am. Chem. Soc. 1983, 105, 4662–4670.
- (33) Geer, A. M.; Julián, A.; López, J. A.; Ciriano, M. A.; Tejel, C. Pseudo-tetrahedral Rhodium and Iridium Complexes: Catalytic Synthesis of *E*-Enynes. *Chem.—Eur. J.* **2018**, *24*, 17545–17556.
- (34) Older, C. M.; Stryker, J. M. Allyl/Alkyne Coupling Reactions Mediated by Neutral Ruthenium(II). Isolation and Characterization of Ruthenium(II)  $\eta^3$ -Allyl  $\eta^2$ -Alkyne Complexes. *Organometallics* **2000**, *19*, 2661–2663.
- (35) Templeton, J. L.; Ward, B. C. Carbon-13 Chemical Shifts of Alkyne Ligands as Variable Electron Donors in Monomeric Molybdenum and Tungsten Complexes. *J. Am. Chem. Soc.* **1980**, 102, 3288–3290.
- (36) Crane, T. W.; White, P. S.; Templeton, J. L. Conversion of Tungsten(IV) Oxo-Alkyne Complexes to Oxo-Vinylidene Complexes. *Organometallics* **1999**, *18*, 1897–1903.
- (37) Crane, T. W.; White, P. S.; Templeton, J. L. Deprotonation of Cationic Tungsten(IV) Aqua—Oxo—Alkyne Complexes To Form Dioxo—Vinyl Tungsten(VI) Complexes. *Inorg. Chem.* **2000**, *39*, 1081—1091.
- (38) Bennett, M. A.; Heath, G. A.; Hockless, D. C. R.; Kovacik, I.; Willis, A. C. Chelate Alkyne Complexes of Divalent and Trivalent Ruthenium Stabilized by N-Donor Ligation. *Organometallics* **1998**, 17, 5867–5873.
- (39) Dutta, B.; Curchod, B. F. E.; Campomanes, P.; Solari, E.; Scopelliti, R.; Rothlisberger, U.; Severin, K. Reactions of Alkynes with [RuCl(cyclopentadienyl)] Complexes: The Important First Steps. *Chem.—Eur. J.* **2010**, *16*, 8400–8409.
- (40) (a) Rummelt, S. M.; Radkowski, K.; Roşca, D.-A.; Fürstner, A. Interligand Interactions Dictate the Regioselectivity of *trans*-Hydrometalations and Related Reactions Catalyzed by [Cp\*RuCl]. Hydrogen Bonding to a Chloride Ligand as a Steering Principle in Catalysis. *J. Am. Chem. Soc.* **2015**, *137*, 5506–5519. (b) Roşca, D.-A.; Radkowski, K.; Wolf, L. M.; Wagh, M.; Goddard, R.; Thiel, W.;

- Fürstner, A. Ruthenium-Catalyzed Alkyne *trans*-Hydrometalation: Mechanistic Insights and Preparative Implications. *J. Am. Chem. Soc.* **2017**, *139*, 2443–2455. (c) Barsu, N.; Leutzsch, M.; Fürstner, A. Ruthenium-Catalyzed *trans*-Hydroalkynylation and *trans*-Chloroalkynylation of Internal Alkynes. *J. Am. Chem. Soc.* **2020**, *142*, 18746–18752.
- (41) Wieder, N. L.; Carroll, P. J.; Berry, D. H. Structure and Reactivity of Acetylene Complexes of Bis(imino)pyridine Ruthenium(0). *Organometallics* **2011**, *30*, 2125–2136.
- (42) Marinelli, G.; Rachidi, I. E.-I.; Streib, W. E.; Eisenstein, O.; Caulton, K. G. Alkyne Hydrogenation by a Dihydrogen Complex: Synthesis and Structure of an Unusual Iridium/Butyne Complex. *J. Am. Chem. Soc.* 1989, 111, 2346–2347.
- (43) Conner, K. M.; Perugini, A. L.; Malabute, M.; Brown, S. N. Group 10 Bis(iminosemiquinone) Complexes: Measurement of Singlet—Triplet Gaps and Analysis of the Effects of Metal and Geometry on Electronic Structure. *Inorg. Chem.* **2018**, *57*, 3272—3286.
- (44) Haungs, D. A.; Brown, S. N. Slicing the  $\pi$  in Three Unequal Pieces: Iridium Complexes with Alkyne, Iminoxolene, and Dioxolene Ligands. *Organometallics* **2022**, *41*, 3612–3626.
- (45) Sanderson, R. T. Principles of Electronegativity. Part I. General Nature. *J. Chem. Educ.* **1988**, *65*, 112–118.
- (46) Feng, S. G.; Philipp, C. C.; Gamble, A. S.; White, P. S.; Templeton, J. L. Synthesis and Characterization of Chiral (Hydridotris(3,5-dimethylpyrazolyl)borato)tungsten(II) Alkyne Complexes. *Organometallics* **1991**, *10*, 3504–3512.
- (47) Brown, S. N.; Mayer, J. M. Photochemical Metal-to-Oxo Migrations of Aryl and Alkyl Ligands. *Organometallics* **1995**, *14*, 2951–2960.
- (48) Conry, R. R.; Mayer, J. M. Rhenium(I) Tris(acetylene) Complexes:  $Re(OR')(RC \equiv CR)_3$  and  $[Re(L)(RC \equiv CR)_3]OTf$ . Organometallics 1993, 12, 3179–3186.
- (49) Hoffman, D. M.; Huffman, J. C.; Lappas, D.; Wierda, D. A. Alkyne Reactions with Rhenium(V) Oxo Alkyl Phosphine Complexes—Phosphine Displacement versus Apparent Re–P Insertion. *Organometallics* **1993**, *12*, 4312–4320.
- (50) Tate, D. P.; Augl, J. M. A Novel Acetylenic Complex of Tungsten(0) Carbonyl. J. Am. Chem. Soc. 1963, 85, 2174–2175.
- (51) Albright, T. A.; Hoffmann, R.; Thibeault, J. C.; Thorn, D. L. Ethylene Complexes. Bonding, Rotational Barriers, and Conformational Preferences. J. Am. Chem. Soc. 1979, 101, 3801–3812.
- (52) Jaroszewski, M.; Szymańska-Buzar, T.; Wilgocki, M.; Ziółkowski, J. J. Photochemical synthesis, spectroscopic properties and barriers to alkene rotation in the novel bis(alkene) tetracarbonyl complexes of tungsten. *J. Organomet. Chem.* **1996**, 509, 19–28.
- (53) Faller, J. W.; Johnson, B. V.; Schaeffer, C. D., Jr. Organometallic Conformational Equilibria. XX. Preferred Orientations and Rotational Barriers of  $\pi$ -Olefins in Chiral Tin-Iron Compounds. The Isolation of Diastereoisomers in Prochiral Olefin Derivatives. *J. Am. Chem. Soc.* **1976**, 98, 1395–1400.
- (54) Harrison, N. C.; Murray, M.; Spencer, J. L.; Stone, F. G. A. Synthesis and Dynamic Behaviour of Bis(ethylene)(tertiary phosphine)-platinum Complexes. *J. Chem. Soc., Dalton Trans.* **1978**, 1337–1342
- (55) Fanizzi, F. P.; Intini, F. P.; Maresca, L.; Natile, G.; Lanfranchi, M.; Tiripicchio, A. Four- *versus* Five-co-ordination in Palladium(II) and Platinum(II) Complexes containing 2,9-Dimethyl-1,10-phenanthroline (dmphen). Crystal Structures of  $[PtCl_2(dmphen)]$  and  $[Pt(\eta^2-C_2H_4)Cl_2(dmphen)]$ . *J. Chem. Soc., Dalton Trans.* **1991**, 1007–1015.
- (56) McNally, J. P.; Cooper, N. J. Mechanism of the Conversion of Intermediate 16-Electron Tungstenocene Alkyls into Alkene Hydrides and Fluxionality within  $[W(\eta^5-C_5H_5)_2(CH_2=CHCH_3)H]PF_6$ . Organometallics 1988, 7, 1704–1715.
- (57) Ward, B. C.; Templeton, J. L. Nuclear Magnetic Resonance Studies of Alkynes as Four-Electron Donor Ligands in Monomeric Tungsten(II) Complexes. J. Am. Chem. Soc. 1980, 102, 1532–1538.

- (58) Badiei, Y. M.; Warren, T. H. Electronic structure and electrophilic reactivity of discrete copper diphenylcarbenes. *J. Organomet. Chem.* **2005**, 690, 5989–6000.
- (59) Herrick, R. S.; Templeton, J. L. Syntheses, Spectral Properties, and Dynamic Solution Behavior of Bis(alkyne)bis(dithiocarbamato)-molybdenum(II) Complexes. *Organometallics* **1982**, *1*, 842–851.
- (60) Fanizzi, F. P.; Natile, G.; Lanfranchi, M.; Tiripicchio, A.; Pacchioni, G. Five-coordinate platinum(II) alkyne complexes: synthesis, ab initio calculations and crystal and molecular structure of  $[PtI_2(Me_2phen)(\eta^2-PhC)] \bullet CHCl_3$ . *Inorg. Chim. Acta* 1998, 275–276, 500–509.
- (61) Alt, H. G. Cyclopentadienyl-Carbonyl-Acetylen-Methyl-Wolfram, Eine Ausgangsverbindung für Neue Wolfram-Acetylen-Komplexe. *J. Organomet. Chem.* **1977**, 127, 349–356.
- (62) Wells, M. B.; White, P. S.; Templeton, J. L. Cyclization Reactions of Coordinated Alkynes in Tungsten(II) Complexes. *Organometallics* **1997**, *16*, 1857–1864.
- (63) Kowalczyk, J. J.; Arif, A. M.; Gladysz, J. A. Synthesis, Structure, and Reactivity of Chiral Rhenium Alkyne Complexes of the Formula  $[(\eta^5-C_3H_5)Re(NO)(PPh_3)(RC \equiv CR')]^+BF_4^-$ . Organometallics 1991, 10, 1079–1088.
- (64) For the A/C designation for the Ru stereocenter, see: Connelly, N. G.; Damhus, T.; Hartshorn, R. M.; Hutton, A. T. Nomenclature of Inorganic Chemistry IUPAC Recommendations 2005; RSC Publishing: Cambridge, UK, 2005.
- (65) Quan, R. W.; Li, Z.; Jacobsen, E. N. Enantiofacially Selective Binding of Prochiral Olefins to a Chiral Catalyst via Simultaneous Face—Face and Edge—Face Aromatic Interactions. *J. Am. Chem. Soc.* **1996**, *118*, 8156—8157.
- (66) Cavallo, L.; Cucciolito, M. E.; De Martino, A.; Giordano, F.; Orabona, I.; Vitagliano, A. Stereoselectivity and Chiral Recognition in Copper(I) Olefin Complexes with a Chiral Diamine. *Chem.—Eur. J.* **2000**, *6*, 1127–1139.
- (67) Cucciolito, M. E.; Jama, M. A.; Giordano, F.; Vitagliano, A.; De Felice, V. 1,2-Diphenyl-*N*,*N*′-bis[(2,4,6-trimethylphenyl)methyl]-1,2-diaminoethane. Stereoselective Coordination of Olefins and Molecular Structure of a Trigonal Bipyramidal Adduct. *Organometallics* 1995, 14, 1152–1160.
- (68) Gladysz, J. A.; Boone, B. J. Chiral Recognition in  $\pi$  Complexes of Alkenes, Aldehydes, and Ketones with Transition Metal Lewis Acids; Development of a General Model for Enantioface Binding Selectivities. *Angew. Chem., Int. Ed. Engl.* **1997**, 36, 550–583.
- (69) Raiford, D. S.; Fisk, C. L.; Becker, E. D. Calibration of Methanol and Ethylene Glycol Nuclear Magnetic Resonance Thermometers. *Anal. Chem.* 1979, 51, 2050–2051.
- (70) Sheldrick, G. M. A short history of SHELX. Acta Crystallogr., Sect. A: Found. Crystallogr. 2008, 64, 112–122.
- (71) Wilson, A. J. C.; Geist, V. International Tables for Crystallography. Vol. C: Mathematical, Physical and Chemical Tables; Kluwer Academic Publishers: Dordrecht/Boston/London, 1992.
- (72) Frisch, M. J.; Trucks, G. W.; Schlegel, H. B.; Scuseria, G. E.; Robb, M. A.; Cheeseman, J. R.; Scalmani, G.; Barone, V.; Petersson, G. A.; Nakatsuji, H.; Li, X.; Caricato, M.; Marenich, A. V.; Bloino, J.; Janesko, B. G.; Gomperts, R.; Mennucci, B.; Hratchian, H. P.; Ortiz, J. V.; Izmaylov, A. F.; Sonnenberg, J. L.; Williams-Young, D.; Ding, F.; Lipparini, F.; Egidi, F.; Goings, J.; Peng, B.; Petrone, A.; Henderson, T.; Ranasinghe, D.; Zakrzewski, V. G.; Gao, J.; Rega, N.; Zheng, G.; Liang, W.; Hada, M.; Ehara, M.; Toyota, K.; Fukuda, R.; Hasegawa, J.; Ishida, M.; Nakajima, T.; Honda, Y.; Kitao, O.; Nakai, H.; Vreven, T.; Throssell, K.; Montgomery, J. A., Jr.; Peralta, J. E.; Ogliaro, F.; Bearpark, M. J.; Heyd, J. J.; Brothers, E. N.; Kudin, K. N.; Staroverov, V. N.; Keith, T. A.; Kobayashi, R.; Normand, J.; Raghavachari, K.; Rendell, A. P.; Burant, J. C.; Iyengar, S. S.; Tomasi, J.; Cossi, M.; Millam, J. M.; Klene, M.; Adamo, C.; Cammi, R.; Ochterski, J. W.; Martin, R. L.; Morokuma, K.; Farkas, O.; Foresman, J. B.; Fox, D. J. Gaussian 16, Revision C.01; Gaussian, Inc.: Wallingford CT, 2016.